Velocity field statistics in homogeneous steady turbulence obtained using a high-resolution direct numerical simulation

Toshiyuki Gotoh[a)]
Department of Systems Engineering, Nagoya Institute of Technology, Showa-ku, Nagoya 466-8555, Japan

Daigen Fukayama
Information and Mathematical Science Laboratory, Inc., 2-43-1, Ikebukuro, Toshima-ku, Tokyo 171-0014, Japan

Tohru Nakano
Department of Physics, Chuo University, Kasuga, Bunkyo-ku, Tokyo 112-8551, Japan

Velocity field statistics in the inertial to dissipation range of three-dimensional homogeneous steady turbulent flow are studied using a high-resolution DNS with up to $N=1024^3$ grid points. The range of the Taylor microscale Reynolds number is between 38 and 460. Isotropy at the small scales of motion is well satisfied from half the integral scale (L) down to the Kolmogorov scale (η). The Kolmogorov constant is 1.64 ± 0.04, which is close to experimentally determined values. The third order moment of the longitudinal velocity difference scales as the separation distance r, and its coefficient is close to 4/5. A clear inertial range is observed for moments of the velocity difference up to the tenth order, between $2\lambda\approx100\eta$ and $L/2\approx300\eta$, where λ is the Taylor microscale. The scaling exponents are measured directly from the structure functions; the transverse scaling exponents are smaller than the longitudinal exponents when the order is greater than four. The crossover length of the longitudinal velocity structure function increases with the order and approaches 2λ, while that of the transverse function remains approximately constant at λ. The crossover length and importance of the Taylor microscale are discussed. © *2002 American Institute of Physics.* [DOI: 10.1063/1.1448296]

I. INTRODUCTION

Kolmogorov studied the statistical laws of a velocity field for small scales of turbulent motion at high Reynolds numbers.[1,2] Two hypotheses were introduced in his theory (hereafter K41 for short): local isotropy and homogeneity exists; and there is an inertial range in the energy spectrum of the flow that is independent of viscosity and large-scale properties at sufficiently high Reynolds numbers. The most prominent conclusion of his theory is the presence of the Kolmogorov spectrum $E(k)=K\bar{\epsilon}^{2/3}k^{-5/3}$ in the inertial range, where $\bar{\epsilon}$ is the average rate of energy dissipation per unit mass and K is a universal constant.

Since K41, there has been a considerable amount of effort made to study the turbulent velocity field statistics in the inertial range, and the energy spectrum has been a central quantity of interest. The Kolmogorov spectrum and constant have been measured in field and laboratory experiments.[3–7] The exponent for the inertial range spectrum is now widely accepted as $-5/3$, with a small correction to account for flow intermittency. The Kolmogorov constant K is between 1.5 and 2. After studying the results of many experiments, Sreenivasan stated that K is 1.62 ± 0.17.[7] The spectral theory of turbulence has also been used to predict the Kolmogorov constant. The value of K is 1.77 when the Lagrangian history direct interaction approximation (LHDIA) is used,[8,9] and 1.72 when the Lagrangian renormalized approximation (LRA) is used.[10,11] These are fully systematic theories that do not contain any *ad hoc* parameters.

Direct numerical simulations (DNSs) of turbulent flows are now performed at higher Reynolds numbers, due to the recent dramatic increase in computational power. In the early 90's, the resolution of DNS reached $N=512^3$ grid points with a Taylor microscale Reynolds number R_λ of $210\sim240$.[12–20] Most high-resolution DNSs have been performed for steady turbulence conditions to achieve high Reynolds numbers and obtain reliable statistics. Although results were reported with R_λ greater than 200, an inertial range spectrum was observed only for the lowest narrow wave number band at which forcing was applied. The Kolmogorov constant was inferred to be about $1.5\sim2$ in Ref. 14 and 1.62 in Ref. 16, but these results are not convincing, due to the insufficient width of the scaling range, anisotropy of the flow field, limited ensemble size, forcing techniques used, and numerical limitations of the simulations.

Intermittency has also attracted the interest of researchers. Since Kolmogorov's intermittency theory (hereafter K62),[21] many theoretical and statistical models of intermittency have been developed.[4,22,23] The scaling exponents of higher order structure functions for velocity differences in the inertial range were studied intensively. Intermittency increases with a decrease in the size of the scales of motion. The small-scale statistics gradually deviate from a Gaussian distribution, and the scaling exponents differ from those predicted by K41.

Experiments at very high Reynolds numbers have been

a)Electronic mail: gotoh@system.nitech.ac.jp

TABLE I. DNS parameters and statistical quantities of the runs. T^{av}_{eddy} is the period used for the time average.

R_λ	N	$k_{\max}$	ν	c_f	Forcing range	T^{av}_{eddy}	E	$\overline{\epsilon}$	L	λ	$\eta(\times 10^{-2})$	K
38	128^3	60	1.50×10^{-2}	1.30	$\sqrt{3}\leqslant k\leqslant\sqrt{12}$	22.6	1.99	1.19	0.891	0.501	4.10	⋯
54	256^3	121	7.00×10^{-3}	0.70	$\sqrt{3}\leqslant k\leqslant\sqrt{12}$	14.9	1.39	0.627	0.829	0.393	2.72	⋯
70	256^3	121	4.00×10^{-3}	0.50	$\sqrt{3}\leqslant k\leqslant\sqrt{12}$	49.7	1.16	0.457	0.785	0.318	1.93	⋯
125	512^3	241	1.35×10^{-3}	0.50	$\sqrt{3}\leqslant k\leqslant\sqrt{12}$	5.52	1.25	0.492	0.744	0.185	0.841	⋯
284	512^3	241	6.00×10^{-4}	0.50	$1\leqslant k\leqslant\sqrt{6}$	3.03	1.96	0.530	1.246	0.149	0.449	1.64
381	1024^3	483	2.80×10^{-4}	0.51	$1\leqslant k\leqslant\sqrt{6}$	4.21	1.74	0.499	1.139	0.0989	0.258	1.63
460	1024^3	483	2.00×10^{-4}	0.51	$1\leqslant k\leqslant\sqrt{6}$	2.14	1.79	0.506	1.150	0.0841	0.199	1.64

performed in the atmospheric boundary layer and in huge wind tunnels, and the measured scaling exponents were found to deviate from K41 scaling.[5,6,24,25,84] However, there have been arguments made about the lack of small-scale flow isotropy and homogeneity in these experiments, which might be affected by the large-scale shear.[25,26]

For experiments at moderate Reynolds numbers under relatively well-controlled laboratory conditions, the width of the scaling range is usually not large enough to determine the scaling exponents precisely. Extended self-similarity (ESS) has been exploited to overcome this difficulty and applied to various turbulent flows in both experiments and DNSs.[28–31] The idea is to measure the scaling exponents of the structure functions when they are plotted against the third order longitudinal structure function, rather than to use the separation distance. The width of the scaling range is longer than that obtained with the usual method at low to moderate Reynolds numbers. The scaling exponents are anomalous, but do agree with those obtained from high Reynolds number experiments up to a certain order.[24,28–31] However, there is no consensus as to why the structure functions give a longer inertial range, or what is missing from the flow statistics as a result. Also, there is no unique way to determine the scaling exponents for the transverse and mixed velocity structure functions, because those higher order structure functions can be plotted against other types of third order structure functions as well as the third order longitudinal structure function.

There also have been arguments about whether the scaling exponents for the longitudinal and transverse structure functions at small scales are equal.[25–27,32–38] Many experiments and DNSs have reported that higher order longitudinal scaling exponents are larger than transverse ones. However, some researchers have argued that the difference is due to deviation from the assumed conditions, such as local homogeneity, isotropy, and the independence of small scales from macroscale parameters. They have suggested that when the Reynolds number becomes large enough, the difference will vanish.[36,37,39,40]

In many aspects of turbulence research, there have been questions posed about the extent to which the local homogeneity and isotropy of the turbulent velocity field are attained. This will affect the small-scale statistics significantly. Recent experimental studies have shown that local isotropy is partially satisfied for lower order moments.[25,26,37] However, it is not sufficient to examine only the conditions assumed in the above studies, and only a limited knowledge of the true flow conditions is available so far.[26,37,38]

A DNS with a sufficiently large grid size provides a better opportunity to examine the points raised above. It has the advantage that any physical quantity can be measured directly without deforming the flow field. In the present study, a series of large scale DNSs have been performed at a high resolution of up to $N=1024^3$ and $R_\lambda=460$.[41–45] The inertial range of the turbulence field has a considerable length, and useful velocity statistics can be extracted such as the Kolmogorov constant, the energy spectrum, velocity structure functions up to the tenth order, their scaling exponents, and probability density functions for velocity differences. To the authors' best knowledge, these are the first DNS data in the inertial range; the data provide new insight into the inertial and dissipation ranges.

The main purposes of the present paper are to describe the statistics of the velocity field in an incompressible steady turbulent flow obtained from the DNS, and to reexamine current knowledge of turbulence, developed since K41. The paper is organized as follows. The numerical aspects of the present DNS are described in Sec. II, and the energy spectrum is examined in Sec. III. The variation of single point quantities and probability density functions (PDFs) with the Reynolds number is discussed in Sec. IV. The isotropy of the second and third order moments of the velocity difference is examined in Sec. V, and the energy budget is examined in terms of the Kármán–Howarth–Kolmogorov equation in Sec. VI. The structure functions and scaling exponents are discussed in Sec. VII. Section VIII presents an analysis of the crossover lengths of the structure functions. Finally, a summary and conclusions are provided in Sec. IX.

II. NUMERICAL SIMULATION

The Navier–Stokes equations are integrated in Fourier space for unit density:

$$\left(\frac{\partial}{\partial t}+\nu k^2\right)\mathbf{u}=\mathbf{P}(\mathbf{k})\cdot\mathscr{F}[\mathbf{u}\times\boldsymbol{\omega}]_{\mathbf{k}}+\mathbf{f}, \tag{1}$$

$$\langle\mathbf{f}(\mathbf{k},t)\mathbf{f}(-\mathbf{k},s)\rangle=\mathbf{P}(\mathbf{k})\frac{F(k)}{4\pi k^2}\delta(t-s), \tag{2}$$

where $\boldsymbol{\omega}$ is the vorticity vector, $\mathbf{P}(\mathbf{k})$ is the projection operator, $\mathscr{F}$ denotes a Fourier transform, and $\mathbf{f}$ is a solenoidal Gaussian random force that is white in time. The spectrum of the random force $F(k)$ is constant over the low wave number band and zero otherwise; the force is normalized as

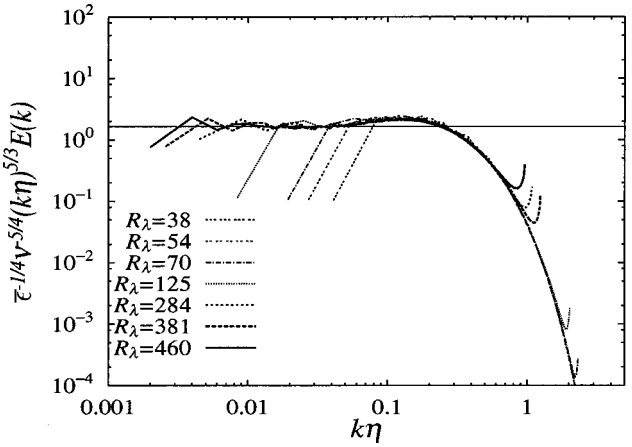

FIG. 1. Scaled energy spectra, $\bar{\epsilon}^{-1/4}\nu^{-5/4}(k\eta)^{5/3}E(k)$. The inertial range is $0.007 \leqslant k\eta \leqslant 0.04$ and $K=1.64\pm0.04$. A horizontal line indicates $K=1.64$.

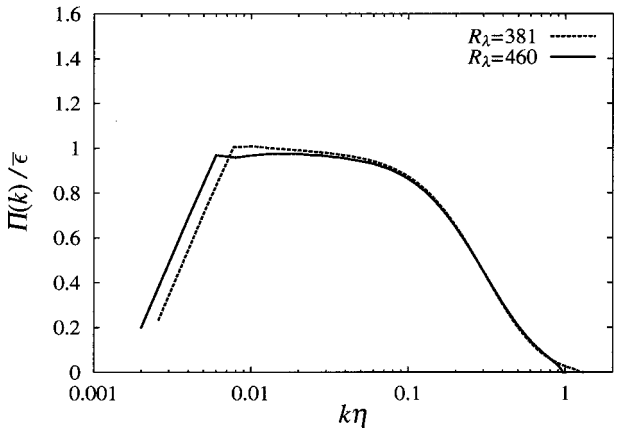

FIG. 2. Normalized energy transfer flux, $\Pi(k)/\bar{\epsilon}$ for $R_\lambda=381$ and 460.

$$\int_0^\infty F(k)dk=\bar{\epsilon}_{in}, \tag{3}$$

where $\bar{\epsilon}_{in}$ is the average rate of the energy input per unit mass. A pseudo-spectral code was used to compute the convolution sums, and the aliasing error was effectively removed. The time integration was performed using the fourth order Runge–Kutta–Gill method.

Physical quantities of turbulent flow include the total energy

$$E(t)=\frac{1}{2}\langle \mathbf{u}^2\rangle=\frac{3}{2}\bar{u}^2=\int_0^\infty E(k)dk, \tag{4}$$

the average energy dissipation per unit mass

$$\bar{\epsilon}=2\nu\int_0^\infty k^2E(k)dk, \tag{5}$$

the integral scale

$$L=\left(\frac{3\pi}{4}\int_0^\infty k^{-1}E(k)dk\right)\Big/ E, \tag{6}$$

the Taylor microscale

$$\lambda=\left(5E\Big/\int_0^\infty k^2E(k)dk\right)^{1/2}, \tag{7}$$

the Taylor microscale Reynolds number

$$R_\lambda=\frac{\bar{u}\lambda}{\nu}, \tag{8}$$

and the Kolmogorov scale

$$\eta=\left(\frac{\nu^3}{\bar{\epsilon}}\right)^{1/4}. \tag{9}$$

The range of the Taylor microscale Reynolds number was 38 to 460. The characteristic parameters of the DNS are listed in Table I.[43] Most of these are identical to Gotoh and Fukayama,[43] but the averaging time for $R_\lambda=381$ was extended to 4.21 large eddy turnover times. A statistically steady state was confirmed by observing the time evolution of the total energy, the total enstrophy, and the skewness of the longitudinal velocity derivative. The statistical averages were computed as time averages over tens of large eddy turnover times for the lower Reynolds number flows, and over a few large eddy turnover times for the higher Reynolds number flows. The resolution condition $k_{\max}\eta>1$ was satisfied for most runs, except for $R_\lambda=460$ in which $k_{\max}\eta$ was slightly less than unity ($k_{\max}\eta=0.96$). This does not adversely affect the results in the inertial range.

The computational time required for runs at a $N=1024^3$ resolution varied, depending on the statistical data that was gathered. Typically, 60 h was required for one large eddy turnover time. The total time of the computations was more than 500 h for the longest run ($R_\lambda=381$). Data collected during the transition period to steady state (about six large eddy turnover times) were discarded. The relatively long time required to attain steady state was due to the low wave number band forcing. This imposes a severe computational restriction. Computations with $R_\lambda \leqslant 284$ were performed on a Fujitsu VPP700E parallel vector machine with 16 processors at RIKEN. Simulations of higher R_λ were performed on a Fujitsu VPP5000/56 with 32 processors at the Nagoya University Computation Center.

III. ENERGY SPECTRUM

Figure 1 shows the three-dimensional energy spectrum calculated for each run. All of the curves are scaled to the Kolmogorov units and multiplied by $k^{5/3}$. As the Reynolds number increases, the curves extend toward lower wave numbers. The curves of flows with Reynolds numbers larger than $R_\lambda=284$ contain a finite plateau, which indicates that $E(k)\propto k^{-5/3}$. There is a bump when $0.04 \leqslant k\eta \leqslant 0.3$ at the high end of the inertial range, which is consistent with previous experimental and numerical observations.[6,16] The normalized energy transfer flux, defined by

$$\frac{1}{\bar{\epsilon}}\Pi(k)=\frac{1}{\bar{\epsilon}}\int_k^\infty T(k')dk' \tag{10}$$

is shown in Fig. 2, where $T(k)$ is a nonlinear energy transfer function in the energy spectrum equation.[4,22] Between $0.007 \leqslant k\eta \leqslant 0.04$, $\Pi(k)/\bar{\epsilon}$ is approximately constant and

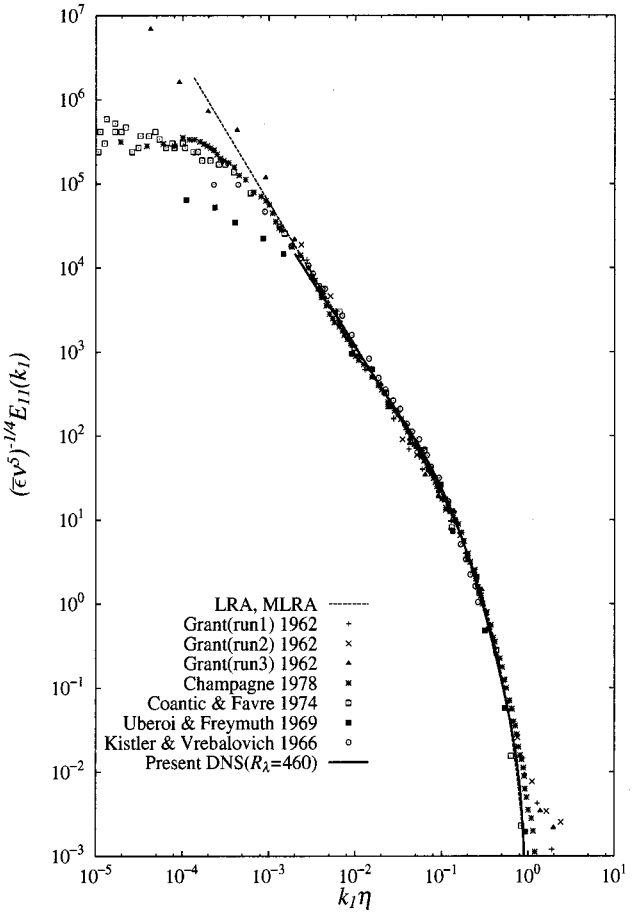

FIG. 3. Comparison of one-dimensional energy spectra. Symbols: experiments, solid line: present DNS ($R_\lambda = 460$), dashed line: statistical theory (LRA and MLRA).

close to unity; thus the flow is in an equilibrium state over the inertial range of the energy spectrum, corresponding to the plateaus in Fig. 1. The Kolmogorov constant given in Table I is determined using a least square fit between $0.007 \leqslant k\eta \leqslant 0.04$ on the $R_\lambda > 284$ curves. In Ref. 43, the Kolmogorov constant was reported as $K = 1.65 \pm 0.05$. However, the averaging time has since been extended for the $R_\lambda = 381$ run. The $R_\lambda = 478$ run differs slightly from statistical equilibrium, since $\Pi(k)/\bar{\epsilon}$ is not exactly one; for this reason, the $R_\lambda = 478$ data were not used for this analysis. The Kolmogorov constant, computed using the data only from the $R_\lambda = 381$ and 460 runs, is

$$K = 1.64 \pm 0.04, \tag{11}$$

which is in good agreement with experimental values and recent DNS data.[7,16] There are many DNSs reporting the Kolmogorov constant higher than the value 1.64. However, the length of the inertial range in those DNSs is not long enough to clearly observe the $k^{-5/3}$ range, and the top of the bump of the compensated energy spectrum $k^{5/3}E(k)$ is understood as the inertial range, so that the Kolmogorov constant is read as about 2 as seen in Fig. 1.[16] The Kolmogorov constant 1.64 is also close to the value obtained using the LHDIA (1.77),[8,9] the LRA (1.72).[10,11] These spectral theories of turbulence are consistent with Lagrangian dynamics, are

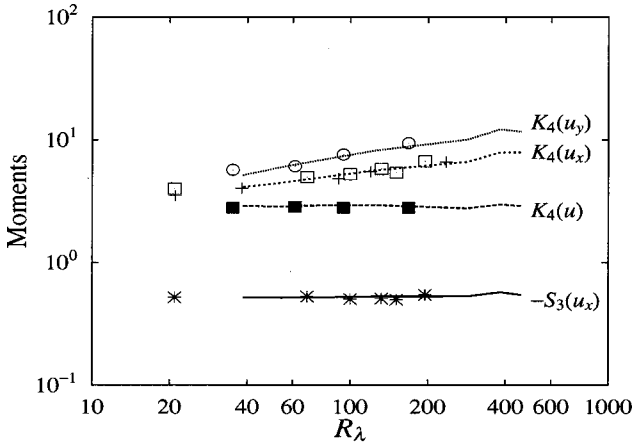

FIG. 4. Variation of the moments of the velocity and velocity gradient with the Reynolds number. Line: present DNS, circle: $K_4(u_y)$ (Jiménez *et al.*, Ref. 13), solid square: $K_4(u)$ (Jiménez *et al.*, Ref. 13), square: $K_4(u_x)$ (Wang *et al.*, Ref. 14), plus: $K_4(u_x)$ (Vedula and Yeung, Ref. 18), star: $-S_3(u_x)$ (Wang *et al.*, Ref. 14).

derived systematically, and contain no *ad hoc* parameters. Figure 3 shows the one-dimensional energy spectrum obtained from the present DNS with $R_\lambda = 460$, from experiments, and from the LRA. The agreement between the curves is satisfactory. Therefore we conclude that the present DNS has successfully calculated a homogeneous turbulent flow field in the inertial range of the energy spectrum.

IV. ONE-POINT STATISTICS

A. Moments

Some one-point moments of the velocity field are

$$S_3(u) \equiv \frac{\langle u^3 \rangle}{\langle u^2 \rangle^{3/2}}, \quad S_3(u_x) \equiv \frac{\langle u_x^3 \rangle}{\langle u_x^2 \rangle^{3/2}}, \tag{12}$$

$$K_4(u) \equiv \frac{\langle u^4 \rangle}{\langle u^2 \rangle^2}, \quad K_4(u_x) \equiv \frac{\langle u_x^4 \rangle}{\langle u_x^2 \rangle^2}, \quad K_4(u_y) \equiv \frac{\langle u_y^4 \rangle}{\langle u_y^2 \rangle^2}, \tag{13}$$

where u is the velocity component in the x direction. The variation of these moments with the Reynolds number is shown in Fig. 4 and listed in Table II. The general behavior of the curves is consistent with previous DNS and experimental data.[13,14,18,19,26,46,47] There are small effects of relatively low resolution on S_3 and K_4 for the velocity derivatives for $R_\lambda = 381$ and 460 data. The skewness factor of the velocity u is very small for runs with the $R_\lambda \leqslant 125$, and is of

TABLE II. Moments of the velocity and velocity derivatives.

R_λ	$S_3(u)$	$K_4(u)$	$S_3(\partial u/\partial x)$	$K_4(\partial u/\partial x)$	$K_4(\partial u/\partial y)$
38	0.0227	2.89	−0.520	4.14	5.16
54	0.00563	2.86	−0.517	4.47	6.00
70	0.00473	2.93	−0.519	4.81	6.62
125	0.0820	2.94	−0.529	5.65	8.19
284	0.0231	2.77	−0.531	6.63	10.1
381	−0.246	2.98	−0.574	7.90	12.2
460	−0.168	2.89	−0.545	7.91	11.7

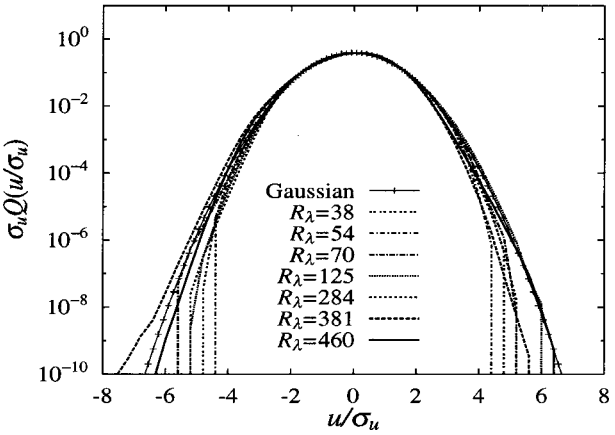

FIG. 5. Variation of velocity PDF with the Reynolds number.

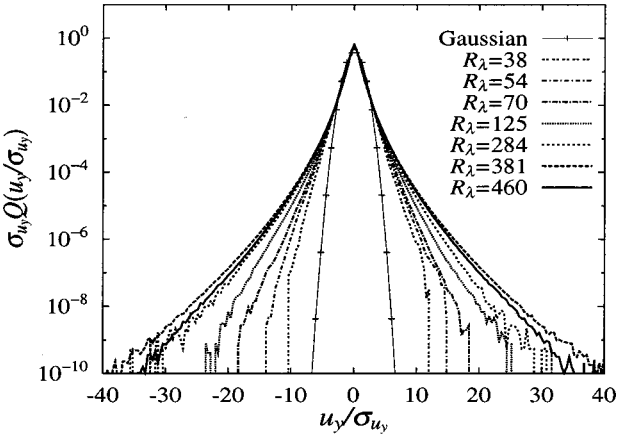

FIG. 7. Variation of the transverse velocity derivative PDF with the Reynolds number.

the order of 0.2 for runs with the $R_\lambda \geqslant 284$. The relatively large values of the velocity skewness are caused by the shorter averaging time used compared to the low Reynolds number runs. Since most of the energy resides in the lowest wave number band, there are persistent large fluctuations of the large scales of motion over longer time period. The longer time average or the forcing at larger wave numbers would yield smaller velocity skewness. The flatness factor of the velocity field is close to three, which is the Gaussian value.

The skewness factor of the longitudinal velocity derivatives is very insensitive to the Reynolds number,

$$S_3(u_x) \propto R_\lambda^{0.0370}, \tag{14}$$

where the exponent is determined by a least square fit. The average value is -0.53, which is consistent with experimental observations over the range of Reynolds numbers studied in the present work. However, the exponent is smaller than indicated by the experimental data.[26,46] The flatness factors for the longitudinal and transverse velocity derivatives increase with the Reynolds number as

$$K_4(u_x) \propto R_\lambda^{0.266}, \quad K_4(u_y) \propto R_\lambda^{0.335}. \tag{15}$$

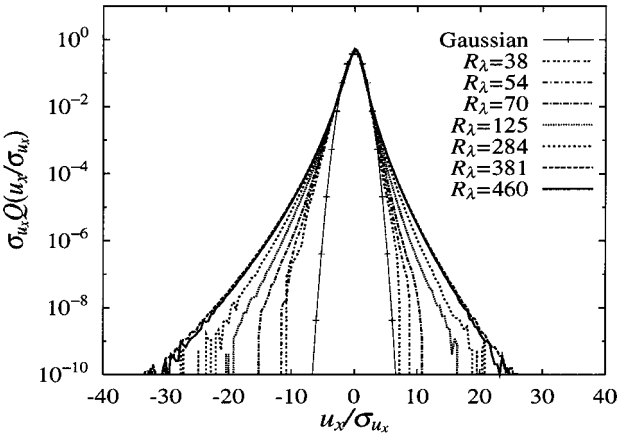

FIG. 6. Variation of the longitudinal velocity derivative PDF with the Reynolds number.

The exponent of $K_4(u_y)$ is larger than that of $K_4(u_x)$; thus, the PDF for the transverse velocity derivative has longer tails than those of the longitudinal velocity derivative. From experimental observations, Shen and Warhaft reported that $K_4(u_x) \propto R_\lambda^{0.37}$ and $K_4(u_y) \propto R_\lambda^{0.25}$.[26] Since there is scatter in the experimetal data, the exponents in Eq. (15) by the present DNS are not inconsistent with the experimental data. Van Atta and Antonia studied the Reynolds number dependence of $S_3(u_x)$ and $K_4(u_x)$,[46] and found that

$$S_3(u_x) \propto R_\lambda^{0.12}, \quad K_4(u_x) \propto R_\lambda^{0.32} \quad \text{for } \mu = 0.2, \tag{16}$$

$$S_3(u_x) \propto R_\lambda^{0.15}, \quad K_4(u_x) \propto R_\lambda^{0.41} \quad \text{for } \mu = 0.25, \tag{17}$$

where μ is the exponent defined by $\langle \epsilon_r^2 \rangle \propto r^{-\mu}$ for the locally averaged energy dissipation rate.[4,21] Generally, the Reynolds number dependency of S_3 and K_4 in our DNSs is weaker than observed in the experiments, irrespective of the type of forcing used. We believe this is because the range of Reynolds numbers in DNS is smaller than experimental flows, and there remain small-scale anisotropy effects in the experiments.

B. Probability density functions

The probability density function conveys information about single-point velocity statistics. It has been one of the central issues of turbulence research in the last decade. Single-point PDFs for the velocity and its derivatives are shown in Figs. 5–7. A longer time period was necessary for the time average to obtain well-converged PDF for the velocity $Q(u)$. The distribution $Q(u)$ is close to Gaussian, and its tail extends to very low values of the order of 10^{-10}. Such values have not been reported in the literature. The $Q(u)$ curve for $R_\lambda = 381$ is skewed negatively, but this is attributed to the insufficient time-averaging period (four large eddy turnover times) that was used. The overall trend is that $Q(u)$ decays faster than a Gaussian distribution at large amplitudes. This behavior was also observed in one-dimensional decaying and forced Burgers turbulence.[48,49]

Jiménez has shown that the PDF $Q(u)$ is slightly sub-Gaussian as the energy spectrum decays faster than k^{-1}.[50]

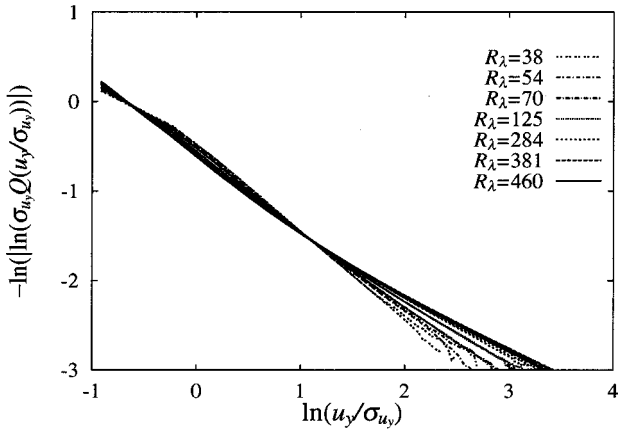

FIG. 8. Variation of the asymptotic tail of the transverse velocity derivative PDF with the Reynolds number. Both positive and negative sides are plotted. The rightmost curve corresponds to $R_\lambda = 460$.

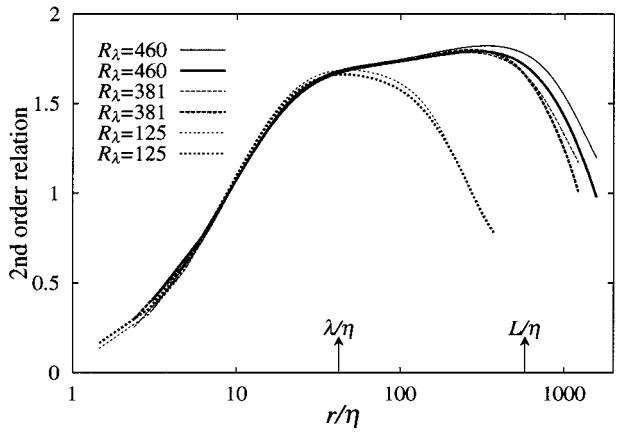

FIG. 9. Isotropy relation at the second order. Thin line: $D_{TT}(r)r^{-2/3}$, thick line: $(D_{LL}(r)+(r/2)(dD_{LL}(r)/dr))r^{-2/3}$. L/η and λ/η are shown for $R_\lambda = 460$.

This is consistent with the present DNS results. Studies of the $Q(u)$ tail predict that $Q(w)\propto\exp(-c|w|^3)$ when the forcing has a short correlation time.[51,52] Here, $w=u/\langle u^2\rangle^{1/2}$ is the normalized velocity amplitude and c is a nondimensional constant. The asymptotic form of $Q(u)$ was examined by plotting $\ln[-\ln(Q(w)]$ against $\ln|w|$; however, the $Q(w)$ tails were too short to determine the true asymptotic form.

The PDF for the longitudinal velocity derivative is slightly skewed, as expected from the finite negative value of the skewness factor. The tail becomes longer as the Reynolds number increases. Figure 7 shows that the PDF of the transverse derivative is symmetric and has a longer tail than the longitudinal derivative.

There are many theories for the PDF of the velocity derivative. The asymptotic tail of $Q(\partial u/\partial y)$ is presented in Fig. 8, in which both the positive and negative sides are plotted by assuming that the PDF is symmetric. The tails gradually become longer as the Reynolds number increases; therefore, $Q(s)$ is Reynolds-number dependent, and cannot be represented in a single stretched exponential form as $Q(s)\propto\exp(-b|s|^h)$, where s is the normalized amplitude of $\partial u/\partial y$ and b is a nondimensional constant that is a function of the Reynolds number.[53]

V. ISOTROPY

The hypothesis of isotropy of the flow field is one of the key components of K41. There are various methods to examine the degree of isotropy. One measure of isotropy can be obtained from the relations between the second and third order longitudinal and transverse velocity structure functions. These are

$$D_{LL}\equiv\langle(\delta u_r)^2\rangle,\quad D_{TT}\equiv\langle(\delta v_r)^2\rangle, \tag{18}$$

$$D_{LLL}\equiv\langle(\delta u_r)^3\rangle,\quad D_{LTT}\equiv\langle\delta u_r(\delta v_r)^2\rangle, \tag{19}$$

where

$$\delta u_r\equiv(\mathbf{u}(\mathbf{x}+\mathbf{r})-\mathbf{u}(\mathbf{x}))\cdot\mathbf{r}/r, \tag{20}$$

$$\delta v_r\equiv(\mathbf{u}(\mathbf{x}+\mathbf{r})-\mathbf{u}(\mathbf{x}))\cdot(\mathbf{I}-\mathbf{rr}/r^2)\cdot\mathbf{e}_\perp, \tag{21}$$

and $\mathbf{e}_\perp$ is the unit vector perpendiculer to $\mathbf{r}$, and $\mathbf{I}$ is the unit tensor. Then the isotropy and incompressibility relations are

$$D_{TT}(r)=D_{LL}(r)+\frac{r}{2}\frac{dD_{LL}(r)}{dr}, \tag{22}$$

$$D_{LTT}(r)=\frac{1}{6}\frac{d}{dr}rD_{LLL}(r). \tag{23}$$

In DNS, the solenoidal property of the Fourier amplitude velocity vector $\mathbf{u}(\mathbf{k})$ is always satisfied to the level of numerical error, which is smaller than 10^{-15}. Thus, the accuracy of the above relations depends solely on the deviation from isotropy. The two sides of Eqs. (22) and (23) are compared for $R_\lambda = 125$, 381, and 460 in Figs. 9 and 10. The curves in the figures are divided by $r^{2/3}$ and r, respectively, and the vertical axes of the plots are linear. The thick lines represent the left hand sides of Eqs. (22) and (23), and the thin lines correspond to the right-hand sides. The isotropy of the second and third order moments is excellent for scales less than $L/2$. The difference at larger separations is caused by the anisotropy due to the small number of energy-containing Fourier modes. The curves for $R_\lambda = 381$ and 460

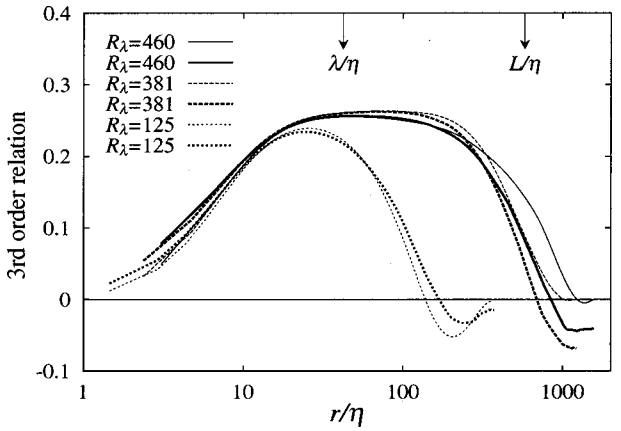

FIG. 10. Isotropy relation at the third order. Thin line: $D_{LTT}(r)r^{-1}$, thick line: $((1/6)(d/dr)rD_{LLL}(r))r^{-1}$. L/η and λ/η are shown for $R_\lambda = 460$.

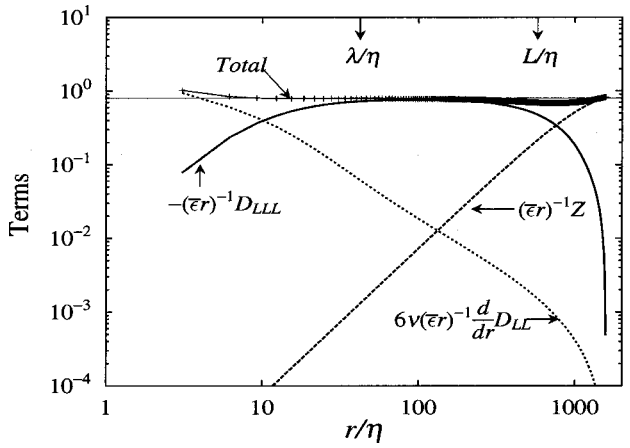

FIG. 11. Terms in the Kármán–Howarth–Kolmogorov equation when $R_\lambda = 460$. Thin solid line: 4/5.

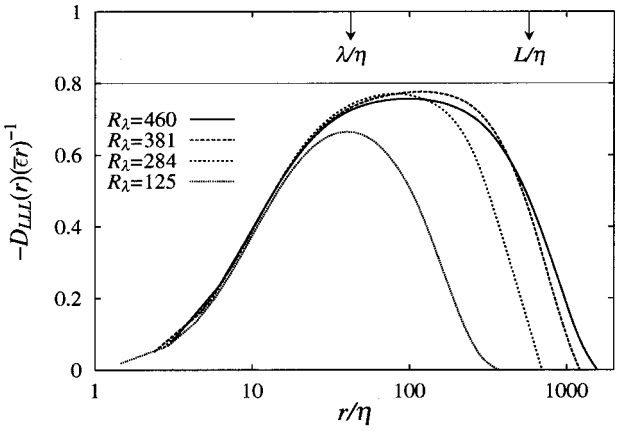

FIG. 12. Kolmogorov's 4/5 law. L/η and λ/η are shown for $R_\lambda = 460$. The maximum values of the curves are 0.665, 0.771, 0.781, and 0.757 for $R_\lambda = 125$, 284, 381, and 460, respectively.

in Fig. 9 are not horizontal, suggesting that the second order structure function does not scale as $r^{2/3}$. The scaling exponents will be examined later in this paper. The isotropic relations, such as $D_{1122}=D_{1133}$ and $D_{2222}=3D_{2233}=D_{3333}$, and Hill's higher order relations were not computed.[54]

VI. KÁRMÁN–HOWARTH–KOLMOGOROV EQUATION

The energy budget for various scales is described by the Kármán–Howarth–Kolmogorov (KHK) equation,

$$\frac{4}{5}\overline{\epsilon}r = -D_{LLL} + 6\nu\frac{\partial D_{LL}}{\partial r} + Z \tag{24}$$

for steady turbulence,[4,55,56] where $Z(r)$ denotes contributions due to the external force given by

$$Z(r,t) = \int_{-\infty}^{t} \langle \delta\mathbf{f}(\mathbf{r},t)\cdot\delta\mathbf{f}(\mathbf{r},s)\rangle ds$$

$$= 12r\int_0^\infty \left(\frac{1}{15} + \frac{\sin kr}{(kr)^3} + 3\frac{\cos kr}{(kr)^4} - 3\frac{\sin kr}{(kr)^5}\right)F(k)dk. \tag{25}$$

Since the external force spectrum $F(k)$ is localized in a range of low wave numbers, the asymptotic form of $Z(r)$ for small separations is given as

$$Z(r) = \frac{2}{35}\overline{\epsilon}_{in}k_f^2 r^3, \quad k_f^2 \equiv \frac{\int_0^\infty k^2F(k)dk}{\int_0^\infty F(k)dk}. \tag{26}$$

A generalized Kármán–Howarth–Kolmogorov equation has also been derived:[57–63]

$$\frac{4}{3}\overline{\epsilon}r = -(D_{LLL}+2D_{LTT}) + 2\nu\frac{\partial}{\partial r}(D_{LL}+2D_{TT}) + W, \tag{27}$$

where

$$W(r) = 4r\int_0^\infty \left(\frac{1}{3} + \frac{\cos kr}{(kr)^2} - \frac{\sin kr}{(kr)^3}\right)F(k)dk,$$

$$\approx \frac{2}{15}\overline{\epsilon}_{in}r^3k_f^2 \quad \text{for } |k_f r| \ll 1. \tag{28}$$

Equation (24) is recovered by substituting Eqs. (22) and (23) into Eq. (27).

Figure 11 shows the results obtained when each term of Eq. (24) is divided by $\overline{\epsilon}r$ for $R_\lambda = 460$. Curves in which r/η is larger than $r/\eta = 1200$ are not shown, because the sign of D_{LLL} changes. A thin horizontal line indicates the Kolmogorov value 4/5. When the separation distance decreases, the effect of the large scale forcing used in the present DNS decreases quickly, while the viscous term grows gradually. The third order longitudinal structure function D_{LLL} quickly rises to the Kolmogorov value, remains there over the inertial range (between $r/\eta \approx 50$ and 300), and then decreases. In the inertial range, the force term decreases as r^3 according to Eq. (26), while the viscous term increases as $r^{\zeta_2-1}(\zeta_2<1)$ when r decreases. [Since each term in the figure is divided by $(\overline{\epsilon}r)$, the slope of each curve is 2 and ζ_2-2, respectively.] The sum of the three terms in the right hand side of Eq. (24) divided by $\overline{\epsilon}r$ is close to 4/5, the Kolmogorov value. The deviation of the sum from the 4/5 law at the smallest scales is due to the slightly lower resolution of the data at these scales ($k_{\max}\eta$ is close to one). At larger scales greater than $r/\eta = 700$, the deviation is caused by the finiteness of the

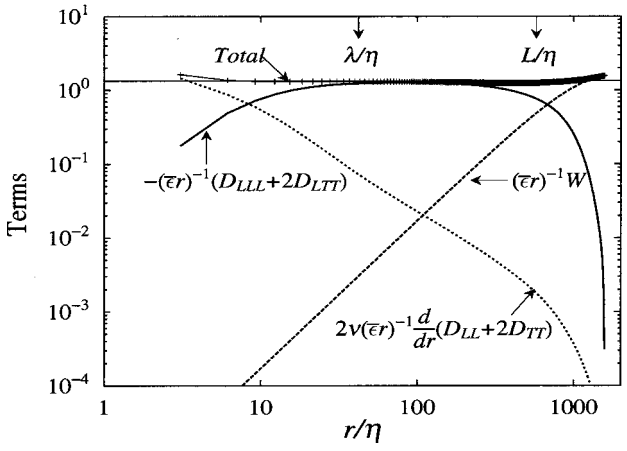

FIG. 13. Terms in the generalized Kármán–Howarth–Kolmogorov equation for $R_\lambda = 460$. Thin solid line: 4/3.

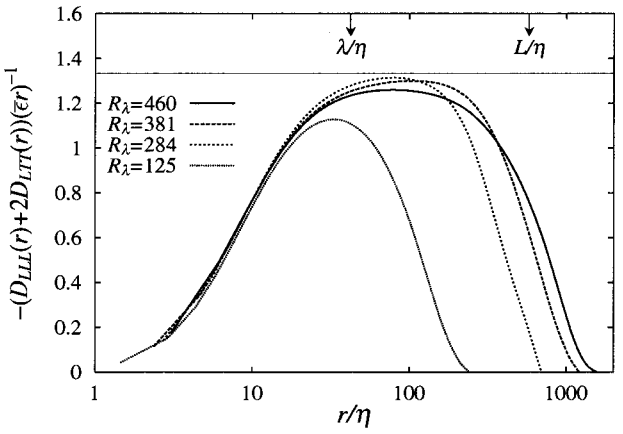

FIG. 14. Kolmogorov's 4/3 law. L/η and λ/η are shown for $R_\lambda=460$. The maximum values of the curves for the 4/3 law are 0.564, 1.313, 1.297, and 1.259 for $R_\lambda=125$, 284, 381, and 460, respectively.

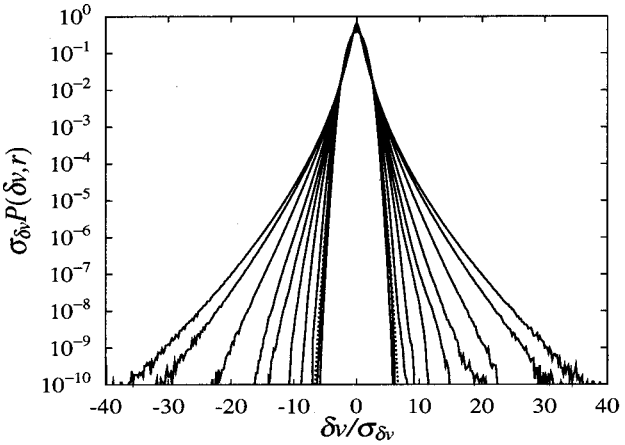

FIG. 16. Variation of PDF for δv_r with r at $R_\lambda=381$. The classification of curves is the same as in Fig. 17.

ensemble, which indicates the persistent anisotropy of the larger scales. The above findings are consistent with the current knowledge of turbulence developed since Kolmogorov, although confirmation of some aspects of turbulence using actual data is new from both a numerical and experimental point of view.[56,59–65]

It is interesting and important to observe when the Kolmogorov 4/5 law is satisfied as the Reynolds number increases.[6,66–69] Figure 12 shows curves of $-D_{LLL}(r)/(\bar{\epsilon}r)$ for various Reynolds numbers. In this figure, the 4/5 law applies when the curves are horizontal. The portion of the curves in which $r/\eta>1200$ is not shown. Although there is a small but finite horizontal range when $R_\lambda>284$, the level of the plateau is still less than the Kolmogorov value. The maximum values of the curves are 0.665, 0.771, 0.781, and 0.757 for $R_\lambda=125$, 284, 381, and 460, respectively. The value 0.781 for $R_\lambda=381$ is 2.5% less than 0.8. An asymptotic state is approached slowly, which is consistent with recent studies. However, the asymptote is approached faster than predicted by the theoretical estimate.[66,69] The slow approach is due to the fact that $D_{LLL}(r)$ is the third order structure function and most positive contributions are canceled by negative ones. Thus only the slight asymmetry of the δu_r PDF contributes to D_{LLL}. The level of the plateau of the $R_\lambda=460$ curve is slightly less than the others. A higher value would be expected if the time average period used for the $R_\lambda=460$ run were longer.

The generalized Kármán–Howarth–Kolmogorov equation Eq. (27) is also examined in a similar fashion. Figure 13 shows each term of the equation divided by $\bar{\epsilon}r$; a horizontal line indicates the 4/3 law. The agreement between the present data and theory is satisfactory. The third order moment slowly approaches the Kolmogorov value 4/3, as shown in Fig. 14. The maximum values of the curves of the 4/3 law are 0.564, 1.313, 1.297, and 1.259 for $R_\lambda=125$, 284, 381, and 460, respectively.

VII. STRUCTURE FUNCTIONS AND SCALING EXPONENTS

The velocity structure functions are defined as

$$S_p^L(r)=\langle|\delta u_r|^p\rangle, \quad S_p^T(r)=\langle|\delta v_r|^p\rangle,$$

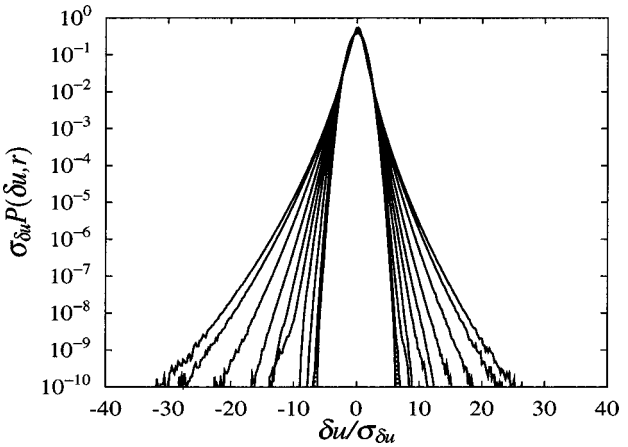

FIG. 15. Variation of the δu_r PDF with r for $R_\lambda=381$. From the outermost curve, $r_n/\eta=2^{n-1}dx/\eta=2.38\times2^{n-1}$, $n=1,...,10$, where $dx=2\pi/1024$. The inertial range corresponds to $n=6$, 7, 8. Dotted line: Gaussian.

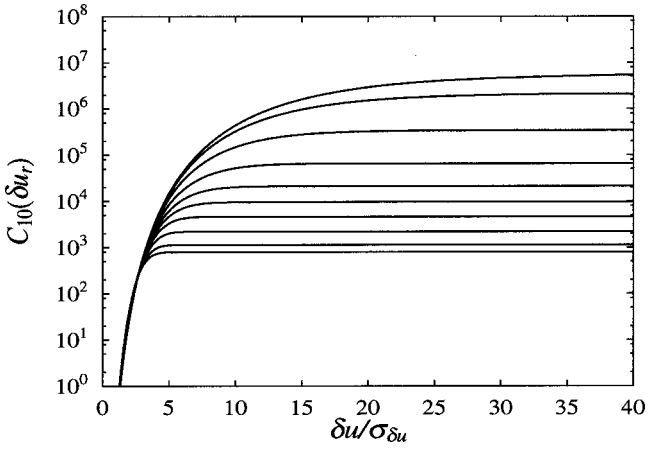

FIG. 17. Convergence of the tenth order accumulated moments $C_{10}(\delta u_r)$ at $R_\lambda=381$ for various separations $r_n/\eta=2.38\times2^{n-1}$, $n=1,...,10$. Curves are for $n=1,...10$ from the uppermost, and the inertial range corresponds to $n=6$, 7, 8.

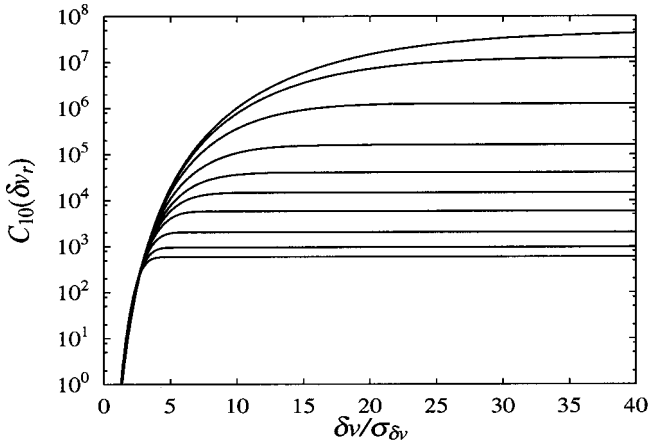

FIG. 18. Convergence of the tenth order accumulated moments $C_{10}(\delta v_r)$ when $R_\lambda = 381$ for various separations r_n/η. The curves are the same as in Fig. 17.

$$S^M_{p,q}(r) = \langle |\delta u_r|^p |\delta v_r|^q \rangle. \tag{29}$$

When the separation is in the inertial range, the structure functions obey the scaling law

$$S^L_p(r) \propto r^{\zeta^L_p}, \quad S^T_p(r) \propto r^{\zeta^T_p}, \quad S^M_{p,q}(r) \propto r^{\zeta^M_{p,q}}. \tag{30}$$

Taking the absolute values of the velocity difference gives well-converged statistics.

The higher the order of the structure functions, the larger the contributions of the PDF tails, so the statistical convergence of higher order structure functions is poor. To increase the statistical ensemble, the velocity structure functions were computed as follows. For a separation vector $r\mathbf{e}_i$, $|\delta u_r(\mathbf{x},s)|^p$ is spatially averaged, then averaged for three directions of the separation vector, and finally averaged over time:

$$\langle |\delta u_r|^p \rangle = \frac{1}{3NT^{av}_{\text{eddy}}} \int_t^{t+T^{av}_{\text{eddy}}} \left(\sum_{i=1}^{3} \sum_{\mathbf{x}} |u(\mathbf{x}+r\mathbf{e}_i, s) - u(\mathbf{x},s)|^p \right) ds, \tag{31}$$

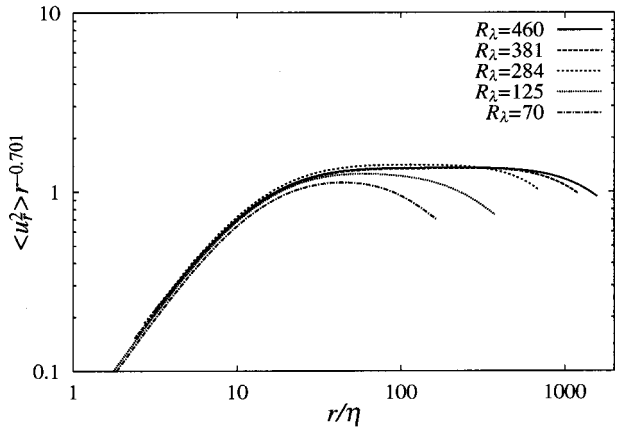

FIG. 19. Plot of $\langle \delta u_r^2 \rangle r^{-0.701}$ against r/η for $R_\lambda = 70$, 125, 284, 381, and 460.

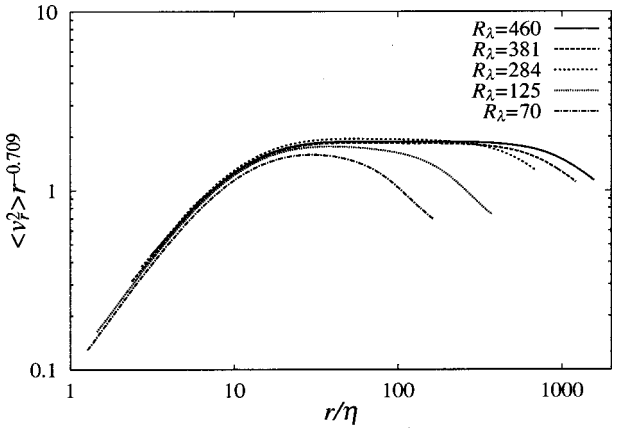

FIG. 20. Plot of $\langle \delta u_r^2 \rangle r^{-0.709}$ against r/η for $R_\lambda = 70$, 125, 284, 381, and 460.

where $\mathbf{e}_i$ is the unit vector in the direction of the x_i axis.

PDFs of the longitudinal and transverse velocity differences when $R_\lambda = 381$ are shown in Figs. 15 and 16 to examine the global change of the velocity difference statistics with respect to scale. As the separation distance decreases, the PDF deviates from a Gaussian distribution and its tail becomes longer. The PDF for the longitudinal velocity increment is skewed negatively, reflecting the energy cascade to smaller scales. However, the PDF for the transverse components is almost symmetric and has a longer tail than the longitudinal PDF. The same trends were observed in the PDFs for $R_\lambda = 460$. Therefore, using the absolute value of the transverse velocity difference is justified in the sense that both positive and negative transverse velocity differences have the same statistics.

The highest order of the structure function for which it is feasible to obtain converged statistics is determined by examining the convergence of the moments of the velocity differences,

$$C_p(z) = \int_0^z |z'|^p Q(z') dz', \tag{32}$$

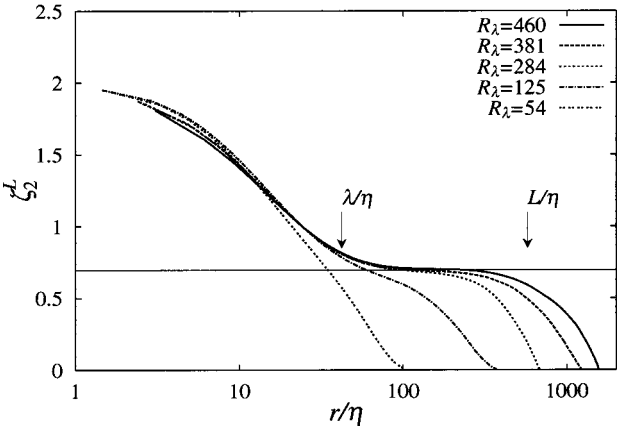

FIG. 21. Variation of the local scaling exponent $\zeta_2^L(r)$ with the Reynolds number. λ/η and L/η for $R_\lambda = 460$ are marked by arrows. A horizontal line shows 0.696.

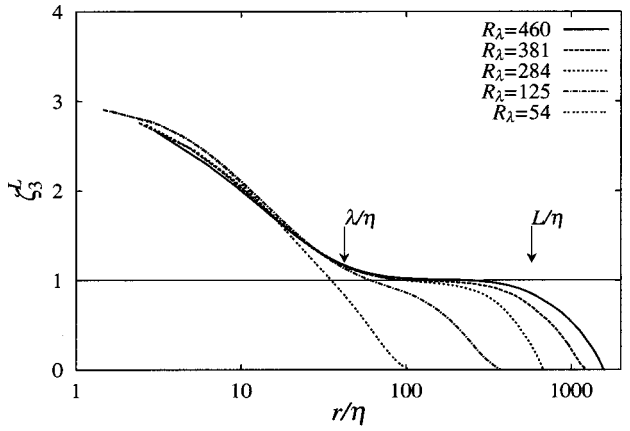

FIG. 22. Variation of the local scaling exponent $\zeta_3^L(r)$ with the Reynolds number. λ/η and L/η for $R_\lambda=460$ are marked by arrows. A horizontal line shows 1.0.

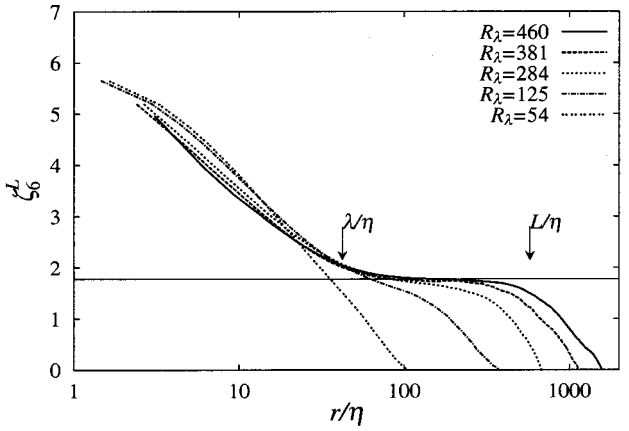

FIG. 24. Variation of the local scaling exponent $\zeta_6^L(r)$ with the Reynolds number. λ/η and L/η for $R_\lambda=460$ are marked by arrows. A horizontal line shows 1.78.

where z is a normalized δu_r or δv_r, and $Q(z)$ is its PDF. Figures 17 and 18 represent $C_{10}(\delta u_r)$ and $C_{10}(\delta v_r)$, respectively. The separation distances are $r_n/\eta=2^{n-1}\,dx/\eta=2.38\times 2^{n-1}$, $n=1,...,10$, where $dx=2\pi/1024$, and the inertial range corresponds to $n=6$, 7, 8. The tenth order structure functions converge well.

Consider first the second order structure functions.[85] As seen in Fig. 9, the curves of $D_{LL}(r)r^{-2/3}$ and $D_{TT}(r)r^{-2/3}$ are not horizontal. The curves of $D_{LL}(r)$ multiplied by $r^{-0.701}$ and $D_{TT}(r)$ multiplied by $r^{-0.709}$ are given in Figs. 19 and 20. In these plots, the exponents are determined using a least square fit. The curves are almost horizontal when $R_\lambda=284$, 381, and 460. The exponent 0.701 is larger than the Kolmogorov value 2/3, but close to the value 0.696 reported by She and Lévêque.[70] The difference $0.701-2/3\approx 0.034$ is small; it is difficult to observe this deviation in the energy spectrum, because the curves are not smooth in wavenumber space (see Fig. 1). One reason that the small intermittency correction to the exponent can be found is that the average of the structure functions is calculated over all the grid points in three directions, yielding an average over a large ensemble (but redundant to some extent). However, only a limited number of Fourier modes are available in the inertial range of the energy spectrum, leading to relatively large fluctuations.

The width of the scaling range of the structure functions increases with the Reynolds number. Figures 21–24 illustrate how the longitudinal local scaling exponent $\zeta_p^L=d\log S_p^L(r)/d\log r$, which is a function of r/η, changes with the Reynolds number. As the Reynolds number increases, a horizontal segment appears in the curve. This segment becomes longer and remains at a constant level, indicating convergence of the scaling exponents with respect to R_λ. (Plots of the eighth to tenth orders are not shown to save space.) A horizontal line inserted in each figure indicates the value reported by She and Lévêque.[70] When $R_\lambda=460$, the range of the constant scaling exponents starts at $r/\eta\approx 100$ (about $2\lambda/\eta$) and ends at $r/\eta\approx 300$ (about $L/2\eta$). The same behavior is also observed for the transverse scaling exponents between $r/\eta\approx 50\approx\lambda/\eta$ and 300.

Figures 25–27 show the structure functions of $S_p^L(r)$, $S_p^T(r)$ and $S_{p,q}^M(r)$ at $R_\lambda=460$. The curves obtained when the separation is greater than $1200r/\eta$ are not shown. For the

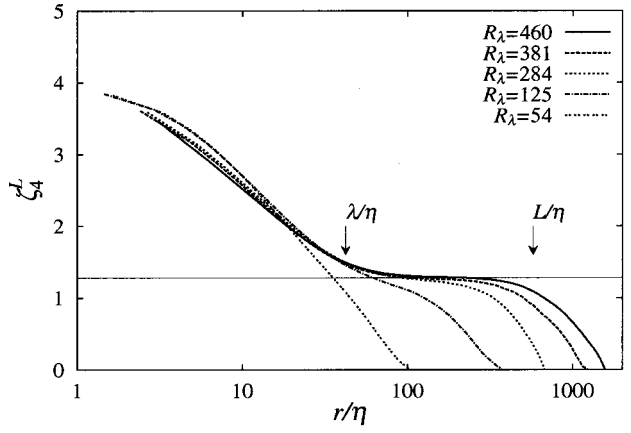

FIG. 23. Variation of the local scaling exponent $\zeta_4^L(r)$ with the Reynolds number. Values of λ/η and L/η for $R_\lambda=460$ are marked by arrows. A horizontal line shows 1.28.

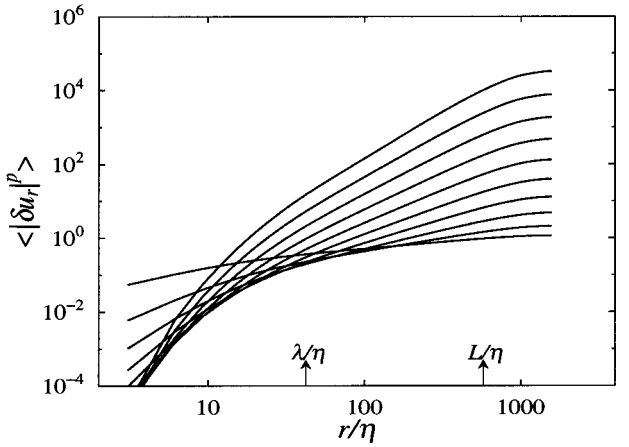

FIG. 25. Plot of $\langle|\delta u_r|^p\rangle$ against r/η for various orders. $R_\lambda=460$. The curves represent $p=1, 2,...,10$ from the lowermost at $r/\eta=L/\eta$.

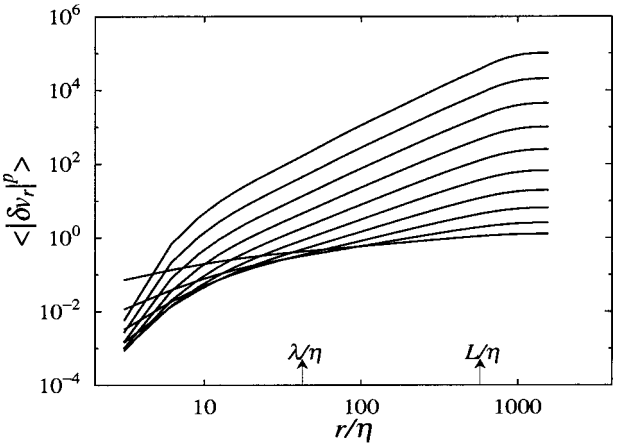

FIG. 26. Plot of $\langle|\delta v_r|^p\rangle$ against r/η for various orders. $R_\lambda=460$. The curves represent $p=1, 2,...,10$ from the lowermost at $r/\eta=L/\eta$.

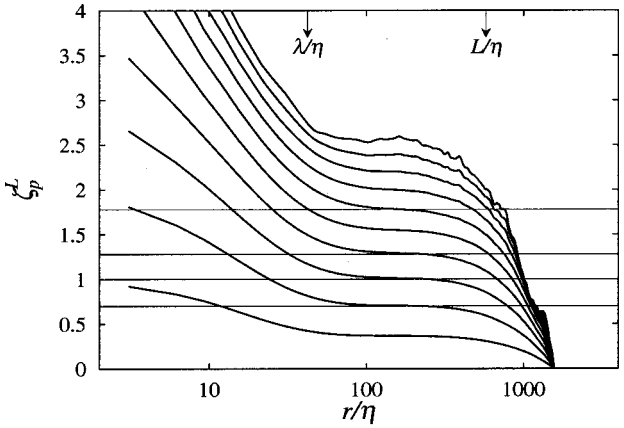

FIG. 28. Variation of the local scaling exponents $\zeta_p^L(r)$ with r/η for various orders. $R_\lambda=460$. The curves represent $p=1, 2,...,10$ (from the lowermost) in the scaling range. Horizontal lines show the values obtained by She and Lévêque, 0.696, 1.0, 1.28, and 1.78.

structure functions at small r, the slope of the curve is approximately p. The curves are straight for separations between λ/η and L/η. The straight portion of $S_p^T(r)$ is slightly longer than that of $S_p^L(r)$, and extends to smaller separations. This can be seen more clearly in plots of the local scaling exponents (see below). The values of $S_p^T(r)$ are larger than those of $S_p^L(r)$. The mixed structure functions for a given order $p+q=2n$ have different slopes: for example, the slope of $S_{6,2}^M(r)$ is larger than that of $S_{4,4}^M(r)$.

The scaling exponents of the structure functions when $R_\lambda=460$ are plotted against the separation distance in Figs. 28–30. Shelves are observed in the curves. These are segments in which the scaling exponents are constant, which is the scaling range of the structure functions. The shelves become narrower as the order increases. Careful examination reveals that:

(1) The scaling range of $S_p^L(r)$ is between $2\lambda/\eta$ and $L/(2\eta)$, while that of $S_p^T(r)$ is between λ/η and $L/(2\eta)$.
(2) Therefore, the scaling range of $S_p^T(r)$ is longer than that of $S_p^L(r)$.
(3) When the order p increases, both the high and low ends of the ζ_p^L shelves move inward, and the scaling range is centered on $r/\eta=200$.
(4) When the order p increases, the high ends of the shelves for ζ_p^T move from $L/(2\eta)$ to a smaller separation, but the low ends stay at λ/η.
(5) The curves of ζ_p^T at higher orders are noisier than those of ζ_p^L.
(6) The average distance of $\zeta_{p+1}^T-\zeta_p^T$ within the scaling range becomes less with the order p faster than that of $\zeta_{p+1}^L-\zeta_p^L$.

Facts (1) to (4) indicate that when the Reynolds number is finite, the width and position of the scaling range of $S_p^T(r)$ differ from those of $S_p^L(r)$. The crossover length at which the scaling behavior of the structure functions ceases due to the effect of the viscosity is also different. As the separation increases from the Kolmogorov scale, the crossover length $l_c(p)$ is defined as the length when $\eta\, d\zeta_p(r)/dr$ exceeds a certain small negative value, say -0.001, for the first time.

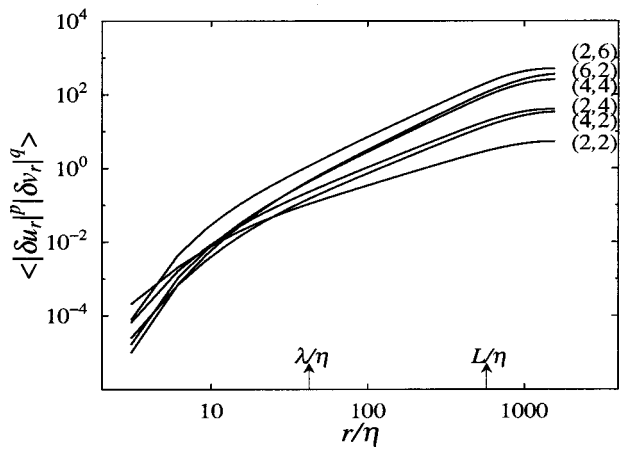

FIG. 27. Plot of $\langle|\delta u_r|^p|\delta v_r|^q\rangle$ against r/η for various orders. $R_\lambda=460$. A set of numbers denotes (p,q).

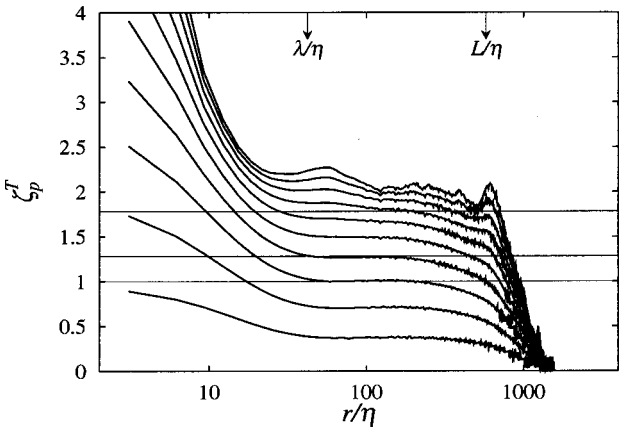

FIG. 29. Variation of the local scaling exponents $\zeta_p^T(r)$ with r/η for various orders. $R_\lambda=460$. The curves represent $p=1, 2,...,10$ (from the lowermost) in the scaling range. Horizontal lines show the values obtained by She and Lévêque, 0.696, 1.0, 1.28, and 1.78.

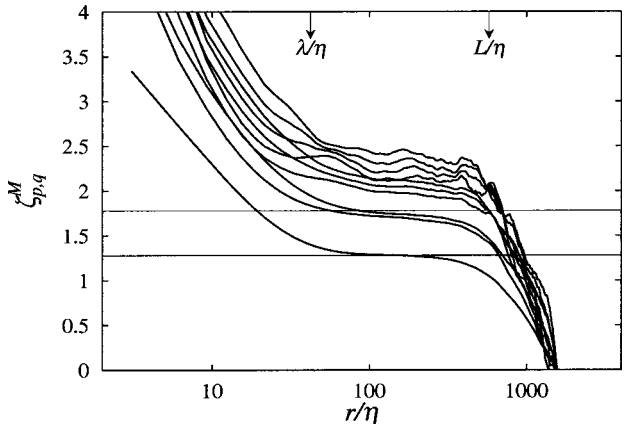

FIG. 30. Variation of the local scaling exponents $\zeta^M_{p,q}(r)$ with r/η for various orders. $R_\lambda=460$. The curves represent $(p,q)=(2,2)$, (4,2), (2,4), (6,2), (4,4), (2,6), (8,2), (6,4), (4,6), (2,8) (from the lowermost) with $r/\eta=200$. Horizontal lines show the values 1.28 and 1.78.

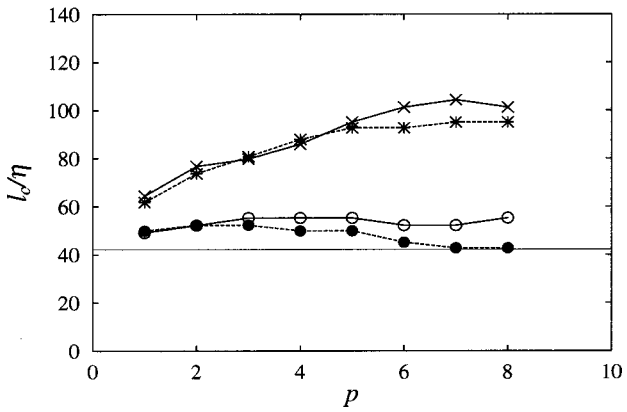

FIG. 31. Variation of the crossover length with the order of the structure functions. Solid line with cross: $l^L_c/\eta(R_\lambda=460)$, solid line with circle: $l^T_c/\eta(R_\lambda=460)$, dashed line with star: $l^L_c/\eta(R_\lambda=381)$, dashed line with filled circle: $l^T_c/\eta(R_\lambda=381)$. A horizontal line indicates λ/η when $R_\lambda=460$.

Figure 31 shows the variation of $l_c(p)/\eta$ for the longitudinal and transverse structure functions. The figure clearly indicates that the crossover length of $S^L_p(r)$ increases with the order and approaches 2λ, while that of $S^T_p(r)$ is λ and approximately independent of the order. The above observation implies that the Taylor microscale is the key length scale at the low end of the scaling range,[71] and is related to the structure of the velocity field. The relatively narrow $\zeta^M_{p,q}$ shelves resemble those of ζ^L_p rather than ζ^T_p. For an order of up to eight,

$$\zeta^T_{2n}<\zeta^M_{2(n-1),2}<\cdots<\zeta^M_{2,2(n-1)}<\zeta^L_{2n} \tag{33}$$

within the scaling ranges of $R_\lambda=381$ and 460. However, the inequalities are weak.

The scaling exponents measured in the scaling range when $R_\lambda=381$ and 460, and the values reported by She and Lévêque, are listed in Table III[70] and plotted in Fig. 32. The DNS values agree with the curves by She and Lévêque up to the sixth order but are slightly smaller at higher order. The curve by the mean field theory by Yakhot is close to the values of ζ^L_p by presnet DNS.[72] Arimitsu and Arimitsu derived analytically the scaling exponents by using the statistics based on the Havrda–Charvat–Tsallis entropy (generalized entropy).[73,74] The theory contains one parameter, the intermittency exponent μ. The results with $\mu=0.25$ are very close to the present DNS results. The present DNS values for $p\geqslant 4$ are slightly larger than the experimental values calculated by Dhruva *et al.*[25] However, the difference is within the error bars, and is probably due to the differing Reynolds numbers of the flow. (The experiments were performed at Reynolds numbers between 10 000 and 15 000.)

There have been many arguments about the appropriate scaling exponents for the longitudinal and transverse exponents.[25–27,32–37,39,40,71,75] Since there are considerable fluctuations, especially in ζ^T_p [see Figs. 28 and 29, and fact (5) above], determination of the scaling exponents at orders larger than six is difficult. These values will have large error bars. The large fluctuations in ζ^T_p indicate that the higher the order of the structure functions, the more the moments are dominated by rare events. Thus, the sample size is smaller, the statistics are less isotropic, and the statistical convergence becomes poorer.

For lower order moments $p\leqslant 3$, the scaling exponents should be equal even when the order is not an integer, since the longitudinal and transverse structure functions are related to each other through Eqs. (22) and (23).

The fourth order moments are related to the second order

TABLE III. Scaling exponents. $\zeta^{SL}_p=p/9+2(1-(2/3)^{p/3})$ is reported by She and Lévêque (Ref. 70). The exponents are determined over the range of r/η: [100,250], [60,200], [100,200] for ζ^L_p, ζ^T_p, and $\zeta^M_{(p,q)}$ when $R_\lambda=381$, and [100,300], [60,200], [100,200] when $R_\lambda=460$, respectively.

	ζ^L_p		ζ^T_p				$\zeta^M_{p,q}$	
p	$R_\lambda=381$	$R_\lambda=460$	$R_\lambda=381$	$R_\lambda=460$	ζ^{SL}_p	(p,q)	$R_\lambda=381$	$R_\lambda=460$
1	0.370±0.004	0.366±0.007	0.369±0.004	0.373±0.013	0.364	(2,2)	1.29±0.01	1.28±0.01
2	0.709±0.009	0.701±0.014	0.701±0.01	0.709±0.013	0.696	(4,2)	1.78±0.02	1.74±0.02
3	1.02 ±0.02	1.01 ±0.02	0.998±0.02	1.01 ±0.01	1.00	(2,4)	1.74±0.03	1.70±0.02
4	1.30 ±0.02	1.29 ±0.03	1.26 ±0.03	1.27 ±0.02	1.28	(6,2)	2.18±0.04	2.12±0.02
5	1.56 ±0.03	1.54 ±0.03	1.49 ±0.04	1.49 ±0.003	1.54	(4,4)	2.14±0.04	2.05±0.02
6	1.79 ±0.04	1.77 ±0.04	1.69 ±0.05	1.67 ±0.04	1.78	(2,6)	2.08±0.04	1.98±0.02
7	1.99 ±0.04	1.98 ±0.06	1.86 ±0.05	1.81 ±0.06	2.00	(8,2)	2.49±0.05	2.43±0.03
8	2.18 ±0.04	2.17 ±0.07	2.00 ±0.04	1.93 ±0.09	2.21	(6,4)	2.46±0.06	2.33±0.03
9	2.35 ±0.04	2.35 ±0.08	2.11 ±0.05	2.02 ±0.13	2.41	(4,6)	2.41±0.04	2.23±0.04
10	2.49 ±0.04	2.53 ±0.09	2.20 ±0.06	2.08 ±0.18	2.59	(2,8)	2.32±0.05	2.14±0.03

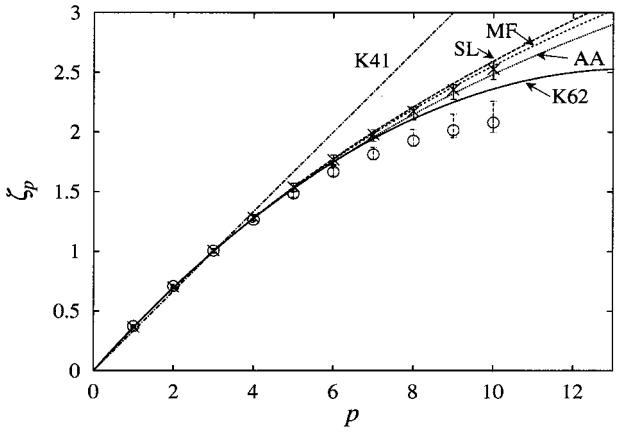

FIG. 32. Variation of the scaling exponents ζ_p^L and ζ_p^T when $R_\lambda=460$. Symbols are the results of the present DNS, star: ζ_p^L, circle: ζ_p^T. SL, MF, AA, and K62 are the curves by She and Lévêque model (Ref. 70), Yakhot's mean field theory (Ref. 72), Arimitsu and Arimitsu's generalized entropy theory with $\mu=0.25$, and K62 with $\mu=0.25$, respectively.

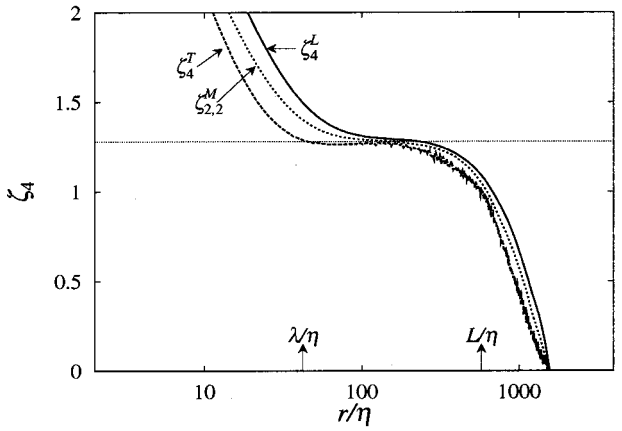

FIG. 34. Comparison of the fourth order scaling exponents ζ_4^L, ζ_4^T, and $\zeta_{2,2}^M$. $R_\lambda=460$. A horizontal line indicates 1.28.

pressure structure function $\langle(\delta_r p)^2\rangle=\langle(p(\mathbf{x}+\mathbf{r})-p(\mathbf{x}))^2\rangle$ through the Poisson kernel.[43,71,75,76] This relation may serve as a constraint among the three structure functions at the fourth order, but it is not restrictive in the sense that there is no direct relation between S_4^L, S_4^T, and $S_{2,2}^M$.[54,72,77,78] Nelkin argued that the pressure spectrum can be expressed in terms of the dissipation spectrum $E^\epsilon(k)=4\pi k^2\mathscr{F}[\langle\epsilon_x\epsilon_{x+r}\rangle]$, the enstrophy spectrum $E^\Omega(k)=4\pi k^2\mathscr{F}[\langle\Omega_x\Omega_{x+r}\rangle]$, and the spectrum of the product of the enstrophy and dissipation $E^M(k)=4\pi k^2\mathscr{F}[\langle\epsilon_x\Omega_{x+r}\rangle]$. He suggested that the three exponents are equal in the limit of high Reynolds numbers.[71,76,87] However, the exponents in the spectra [for example, μ^ϵ in $E^\epsilon(k)=C^\epsilon\overline{\epsilon^2}k^{-1}(kL)^{-\mu^\epsilon}$] are not necessarily equal to those of $S_4^L(r)$, $S_4^T(r)$, or $S_{2,2}^M(r)$. The former are the spectra of the dissipation range quantities, while the latter are the fourth order correlations of inertial range quantities.

The DNS values of the scaling exponents are $\zeta_4^T=1.27$, $\zeta_{2,2}^M=1.28$, and $\zeta_4^L=1.29$ for $R_\lambda=460$ which are obtained by averaging over the scaling range. The difference between these values is within 3%. Figures 33 and 34 show the variation of the fourth order scaling exponents with separation distance for two Reynolds numbers. At the high end of the r range, the difference between the exponents is less. Although it is again difficult to draw definite conclusions from the figures, it seems that the differences between the three scaling exponents decrease with the Reynolds number.[71]

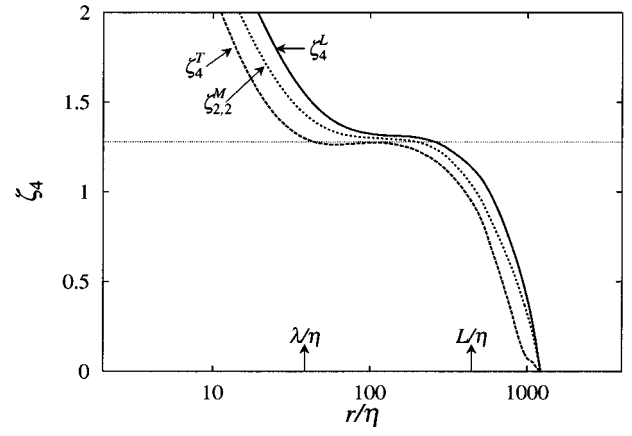

FIG. 33. Comparison of the fourth order $\zeta_{2,2}^M$. $R_\lambda=381$. A horizontal line indicates 1.28.

For higher order moments $p>4$, there are no simple equations to directly relate the longitudinal and transverse structure functions. A dynamical equation relates different types of structure functions at various orders.[54,72,77,78] L'vov *et al.* have pointed from the view point of the irreducible representation of the rotation symmetry group that the longitudinal and transverse structure functions must have the same asymptotic scaling exponents for infinite Reynolds number, but different exponents can be observed when the scaling range is not long enough.[39] He *et al.* discussed that the scaling exponents for locally averaged enstrophy and dissipation are equal for infinite Reynolds number, but may be different for finite Reynolds number.[40] From this argument, they suggested that the scaling exponents for the longitudinal and transverse structure functions are also equal at infinite Reynolds numbers. Zhou and Antonia suggested that the difference $\Delta\zeta_p=\zeta_p^L-\zeta_p^T$ vanishes at sufficiently large Reynolds numbers.[37] However, the present data indicate that the difference $\Delta\zeta_p$ for $R_\lambda=381$ and 460 is larger than the value $\Delta\zeta_p$ extrapolated from the experimental data. The exponents in Table III and Fig. 32 are average values over the entire scaling range and indicate $\zeta_p^T<\zeta_p^L$ for $p>4$. The overall trend of the local scaling exponents within the scaling range suggests that the rate of the increase of ζ_p^T with respect to the order is slower than that of ζ_p^L [fact (6)]. Although the asymptotic state is beyond the scope of the present DNS study, the above observations and facts suggest that ζ_p^T is smaller than ζ_p^L when $p>4$. If some portion of this difference at higher orders arises from the insufficient degree of isotropy, a longer time average would provide insights into this problem. If other portion of the difference comes from the insufficient length of the scaling range, it is necessary to extend farther the scaling range even when we use the invariant scalar func-

tions associated with the higher order velocity tensors, which requires far more computational resources.

VIII. CROSSOVER LENGTH

The scaling behavior of the velocity structure function for a turbulent flow has been examined in detail inspired with the success of statistical physics of phase transitions. The density structure function was introduced there to study the structure of matter using photon, neutron, and electron scattering. The interaction potential between the molecules, the crystal and fractal structure of the matter were obtained from the techniques. Therefore, scaling exponents and other physical quantities should be extracted from the velocity structure functions to provide more information about the turbulent flow. In this section, the physical meaning of the crossover length is considered on the basis of the structure of the flow field.

It is useful to review the scaling exponents of velocity structure functions for the one-dimensional Burgers turbulence. The scaling exponent of the one-dimensional Burgers turbulence is[79,80]

$$\zeta_p = \begin{cases} 1 & \text{for} \quad p \geqslant 1, \\ p & \text{for} \quad p < 1. \end{cases} \tag{34}$$

The nonlinearity balances the viscous term and produces shock waves. Thus, the velocity field resembles a sawtooth wave, with random magnitudes and intervals of shocks. When $p<1$, the contribution to the structure function occurs in the ramp of the sawtooth wave, in which the velocity field is smooth and linear in r; therefore $\zeta_p = p$. The shocks dominate the structure function when $p \geqslant 1$. In this case, the shock is so sharp that it has a definite length scale $l_s = \Delta u/\nu$, where Δu is the velocity jump across the shock. Since the probability of finding a shock within a distance r is proportional to r, and the amplitude of the moment is given by the velocity jump across the shock front, $\langle \delta u_r^p \rangle = \int \delta u^p Q(\delta u, r) d(\delta u)$, it follows that $\zeta_p = 1$ and the crossover occurs at the length of the shock width, i.e., $l_c \approx \langle l_s \rangle \approx u_{\mathrm{rms}}/\nu$, which is independent of the order. Structure functions have been calculated previously up to the twentieth order from a DNS of decaying Burgers turbulence (Fig. 5 in Ref. 80). The scaling was described by Eq. (34), and the crossover length was independent of the order. The most important point of this analysis is that the singularity is very sharp and has a definite shape and length.

Now consider the transverse structure function in Navier–Stokes turbulence. The crossover length of $S_p^T(r)$ is independent of the order, which strongly suggests that there exists a structure with a definite length (approximately λ) in the velocity field. Such structures could be a shear layer of thickness λ or a vortex tube of radius λ. When the separation vector $\mathbf{r}$ encompasses such objects and r is greater than λ, the $S_p^T(r)$ when $p \geqslant 1$ begins to attain the scaling behavior. The scaling exponent ζ_p^T is determined by the velocity amplitudes at the end points of the separation vector and the population of such structures that are governed by the flow dynamics.

The behavior of the longitudinal structure function is slightly different. For a given separation r, most of the contributions to $S_p^L(r)$ come from the regions of flow containing large negative gradients of $\partial u/\partial x$ when $p>1$.[64] The portion of the fluid in which $\delta u_r > 0$ is stretched, and portion in which $\delta u_r < 0$ is compressed in the direction of the separation vector. This is accompanied by squeezing or stretching of ambient fluid on a plane normal to the separation vector, due to pressure action and the incompressibility of the flow. Thus the velocity field is less singular than in the case of Burgers turbulence. The resulting field has a ramp structure, but no shocks occur. For the ramp structure, a linear dimension of a large negative gradient domain $\partial u/\partial x$, say l_*, would be determined by the balance between the convection and the pressure gradient. This differs from Burgers turbulence, in which the shock width is determined by $\Delta u/\nu$. Since the pressure gradient is a function of velocity, the dependence of l_* on velocity indicates that the converse also applies: $\delta u_r(<0)$ depends on l_*. A large order p samples large $\delta u_r(<0)$ and large pressure gradients; therefore, the balance between these quantities results in an l_* that increases slowly with p and saturates at certain distance (about 2λ). This explains the gradual increase of the crossover length with the order. Although the above scenario requires a mathematical analysis,[81,82] it seems plausible that the essential difference between the longitudinal and transverse velocity difference is that the incompressibility condition directly constrains the former, whereas the constraint is only secondary for the latter.

These findings suggest that the Taylor microscale λ is a characteristic length that indicates the low end of the scaling range in real space. This length scale contains more of the physics of the Navier–Stokes dynamics than the Kolmogorov length in the scaling range.

A Burgers vortex consists of a strong vortex core surrounded by a dissipation field. A similar structure is observed in homogeneous isotropic turbulence data from a DNS with a diameter of approximately 10η.[83] However, $\lambda \approx 50\eta$ is five times the diameter of the structure, and 2λ is even longer.[86] This suggests that *the objects that attain the scaling law are those far outside the strong vortex cores and/or shear layers*. This contrasts with the view that turbulence consists of many thin vortex tubes or filaments, as frequently observed in DNS visualizations of regions with high vorticity. Objects in the scaling range are less definitive and have more extended structures. If the strong vortex tubes are the sinews of turbulence, the fluid objects in the inertial range would be the muscles of turbulence. They stretch and/or compress the sinews (strong vortices).

IX. SUMMARY AND DISCUSSION

The velocity field statistics of incompressible steady turbulent flow have been studied using a high-resolution DNS with up to $N=1024^3$ grid points. The range of the Taylor microscale Reynolds number was between 38 and 460. Generally, the results are consistent with previous findings, but the quantitative data are more precise and accurate. This provides new insights into turbulence.

The energy spectra agree well with experimental data, and the inertial range spectrum is clearly observed for the

first time. The Kolmogorov constant is 1.64, consistent with experimental values. The values of the moments of velocity and velocity derivatives and their PDFs are consistent with other DNS and experimental values, but their R_λ dependence is generally weaker than observed in experiments. The tails of PDFs were compared to theoretical predictions, but no definite conclusions were obtained.

The isotropy of the second and third order structure functions is well satisfied for scales of motion below half of the integral scale, which is the upper limit of the inertial range in the present DNS. The energy budgets were examined in terms of the (generalized) Kármán–Howarth–Kolmogorov equation. The energy balance is also satisfied for every scale below the integral scale provided that the time average is sufficient. The Kolmogorov 4/5 and 4/3 laws are almost achieved, but convergence with Reynolds number is slow.

The Reynolds numbers of the flow in the present DNS are lower than those of experiments. However, the degree of isotropy in the present data is very satisfactory compared to the experiments, which requires the Reynolds number to be high enough to obtain local isotropy at small scales. The isotropy of the velocity field in the present DNS is very close to the textbook description, although it is not perfect.[25,32]

There are many reports in the literature stating that the inertial range, or more generally the scaling range, begins at $a\times\eta$ where a is between 10 and 20. This estimate seems reasonable from the point of view of the structure function alone. However, when the local scaling exponents are examined, the true scaling range for δu_r starts at 100η, or about 2λ, which is longer than the estimated length. The present DNS data show that the strength of the inequality over the inertial range, usually defined as $\eta\ll r\ll L$, indicates that 100 times η is at the low end. This agrees with the textbook theory. On the other hand, the upper end of the scaling range is L/b, where b is of order of unity, provided that the forcing is applied in the low wavenumber range and that the sample size is large enough to satisfy isotropy. Therefore, as far as the qualitative features of the lower order statistics such as the local homogeneity, isotropy, and energy budgets are concerned, the K41 theory of turbulence is correct provided that the large scale forcing is well controlled. However, there certainly exist deviations in the statistics from the K41 predictions for every order except that of the 4/5 law, even under idealized conditions at large scales.

The convergence of the scaling exponents of the structure functions with the Reynolds number is examined and found to be satisfactory up to the tenth order for both the longitudinal and transverse velocity differences. The scaling exponents are directly measured as functions of separation. The exponents $\zeta_2^L=0.701\pm0.014$ and $\zeta_2^T=0.709\pm0.013$ are very close to each other and larger than the Kolmogorov value, 2/3. Equation (22) indicates that the two exponents must be equal. The small difference (1%) is due to the finite sample size and small amount of flow anisotropy. Since small differences remain in the scaling exponents, even at the second order, determining the precise values of the exponents is very difficult. The higher order scaling exponents are definitely anomalous and increase slower than predicted by the K41 scaling theory. The ζ_p^T exponent is smaller than ζ_p^L when $p>4$, but no definite conclusions can be made, since a larger ensemble and longer scaling range are required.

Careful examination shows that the scaling ranges of the longitudinal and transverse structure functions are different. The crossover length of $S_p^L(r)$ is longer than that of $S_p^T(r)$, increases with the order, and then approaches 2λ. The crossover length of $S_p^T(r)$ is λ and approximately independent of the order. This difference is due to the structure of the turbulence field characterized by the Taylor microscale, and suggests that the objects that obey the scaling law are those that are longer than 2λ.

The present method of determining the scaling exponents is more straightforward than ESS. Although the width of scaling range obtained using the present method is not as long as that of ESS, the results indicate that the crossover length changes with the order and behaves differently for the longitudinal and transverse structure functions. This could not be determined with ESS. The difference in the position of the scaling ranges of $S_p^L(r)$ and $S_p^T(r)$ raises a question about the relevance of ESS, especially when used to find the scaling exponents of $S_p^T(r)$ in terms of $S_3^L(r)$. This point requires more careful examination.

DNS of turbulence has now reached the point where the inertial range statistics can be obtained directly. This provides a powerful tool and valuable data for turbulence research. There are many aspects not addressed here: for example, the behavior of velocity difference PDFs, the relations amongst various structure functions, the conditional averages of terms in the Navier–Stokes equations, the pressure statistics, etc. These are the goals of future high resolution DNS research of turbulent flows.

ACKNOWLEDGMENTS

The authors are grateful to T. Ochiai and S. Wada for their assistance of the computation. They thank T. Arimitsu, N. Arimitsu, T. Lundgren, J. Qian, Z. Warhaft, V. Yakhot, and P. K. Yeung for their comments and discussions. The authors wish to thank the Nagoya University Computation Center and the Advanced Computing Center at RIKEN for providing the computational resources. This work was supported by a Grant-in-Aid for Scientific Research (C-2 12640118) from the Japan Society for the Promotion of Science.

[1] A. N. Kolmogorov, "The local structure of turbulence in incompressible viscous fluid for very large Reynolds numbers," Dokl. Akad. Nauk SSSR **30**, 9 (1941).
[2] A. N. Kolmogorov, "Dissipation of energy in locally isotropic turbulence," Dokl. Akad. Nauk SSSR **32**, 16 (1941).
[3] H. L. Grant, R. W. Stewart, and A. Moilliet, "Turbulence spectra from a tidal channel," J. Fluid Mech. **12**, 241 (1962).
[4] A. S. Monin and A. M. Yaglom, *Statistical Fluid Mechanics*, Vol. II (MIT Press, Cambridge, 1975).
[5] A. Praskovsky, "Experimental verification of the Kolmogorov refined similarity hypothesis," Phys. Fluids A **4**, 2589 (1992).
[6] S. G. Saddoughi and S. V. Veeravalli, "Local isotropy in turbulent boundary layers at high Reynolds number," J. Fluid Mech. **268**, 333 (1994).
[7] K. R. Sreenivasan, "On the universality of the Kolmogorov constant," Phys. Fluids **7**, 2778 (1995).
[8] R. H. Kraichnan, "Lagrangian-history closure approximation for turbulence," Phys. Fluids **8**, 575 (1965).

[9]R. H. Kraichnan, ''Isotropic turbulence and inertial-range structure,'' Phys. Fluids **9**, 1728 (1966).
[10]Y. Kaneda, ''Renormalized expansions in the theory of turbulence with the use of the Lagrangian position function,'' J. Fluid Mech. **107**, 131 (1981).
[11]Y. Kaneda, ''Inertial range structure of turbulent velocity and scalar fields in a Lagrangian renormalized approximation,'' Phys. Fluids **29**, 701 (1986).
[12]S. Chen, G. D. Doolen, R. H. Kraichnan, and Z. She, ''On statistical correlations between velocity increments and locally averaged dissipation in homogeneous turbulence,'' Phys. Fluids A **5**, 458 (1993).
[13]J. Jiménez, A. A. Wray, P. G. Saffman, and R. S. Rogallo, ''The structure of intense vorticity in isotropic turbulence,'' J. Fluid Mech. **255**, 65 (1993).
[14]L. P. Wang, S. Chen, J. Brasseur, and J. C. Wyngaard, ''Examination of hypothesis in the Kolmogorov refined turbulence theory through high-resolution simulations, Part I. Velocity field,'' J. Fluid Mech. **309**, 113 (1996).
[15]I. Hosokawa, S. Oide, and K. Yamamoto, ''Isotropic turbulence: Important differences between true dissipation rate and its one-dimensional surrogate,'' Phys. Rev. Lett. **77**, 4548 (1996).
[16]P. K. Yeung and Y. Zhou, ''On the universality of the Kolmogorov constant in numerical simulation of turbulence,'' Phys. Rev. E **56**, 1746 (1997).
[17]N. Cao, S. Chen, and G. D. Doolen, ''Statistics and structures of pressure in isotropic turbulence,'' Phys. Fluids **11**, 2235 (1999).
[18]P. Vedula and P. K. Yeung, ''Similarity scaling of acceleration and pressure statistics in numerical simulations of isotropic turbulence,'' Phys. Fluids **11**, 1208 (1999).
[19]T. Gotoh and R. S. Rogallo, ''Intermittency and scaling of pressure at small scales in isotropic forced turbulence,'' J. Fluid Mech. **396**, 257 (1999).
[20]T. Gotoh and K. Nagaya, ''On universality of statistics of pressure field in homogeneous turbulence,'' *Proceedings of IUTAM Symposium on Geometry and Statistics of Turbulence*, edited by T. Kambe (Kluwer, New York, 2001).
[21]A. N. Kolmogorov, ''A refinement of previous hypothesis concerning the local structure of turbulence in a viscous incompressible fluid at high Reynolds number,'' J. Fluid Mech. **13**, 82 (1962).
[22]U. Frisch, *Turbulence: The Legacy of A. N. Kolmogorov* (Cambridge University Press, Cambridge, 1995).
[23]M. Nelkin, ''Universality and scaling in fully developed turbulence,'' Adv. Phys. **43**, 143 (1994).
[24]F. Anselmet, Y. Gagne, E. J. Hopfinger, and R. A. Antonia, ''Higher-order velocity structure functions in turbulent shear flows,'' J. Fluid Mech. **140**, 63 (1984).
[25]B. Dhruva, Y. Tsuji, and K. R. Sreenivasan, ''Transverse structure functions in high Reynolds numbers turbulence,'' Phys. Rev. E **56**, R4928 (1997).
[26]X. Shen and Z. Warhaft, ''The anisotropy of the small scale structure in high Reynolds number ($R_\lambda \sim 1000$) turbulent shear flow,'' Phys. Fluids **12**, 2976 (2000).
[27]X. Shen and Z. Warhaft, ''Longitudinal and transverse structure functions in sheared and unsheared wind-tunnel turbulence,'' Phys. Fluids **14**, 370 (2002).
[28]R. Benzi, S. Ciliberto, R. Tripiccione, C. Baudet, F. Massaioli, and S. Succi, ''Extended self-similarity in turbulent flows,'' Phys. Rev. E **48**, R29 (1993).
[29]R. Benzi, S. Ciliberto, C. Baudet, and G. R. Chavarria, ''On the scaling of three-dimensional homogeneous and isotropic turbulence,'' Physica D **80**, 385 (1995).
[30]M. Briscolini, P. Santangelo, S. Succi, and R. Benzi, ''Extended self-similarity in the numerical simulation of three dimensional homogeneous flows,'' Phys. Rev. E **50**, R1745 (1994).
[31]L. Stolovitzky and K. R. Sreenivasan, ''Scaling of structure functions,'' Phys. Rev. E **48**, R33 (1993).
[32]O. N. Boratav, ''On longitudinal and lateral moment hierarchy in turbulence,'' Phys. Fluids **9**, 3120 (1997).
[33]S. Chen, K. R. Sreenivasan, M. Nelkin, and N. Cao, ''A refined similarity hypothesis for transverse structure functions,'' Phys. Rev. Lett. **79**, 2253 (1997).
[34]O. N. Boratav and R. B. Pelz, ''Structures and structure functions in the inertial range of turbulence,'' Phys. Fluids **9**, 1400 (1997).
[35]W. Van de Water and J. A. Herweijer, ''High-order structure functions of turbulence,'' J. Fluid Mech. **387**, 3 (1999).
[36]G. He, G. D. Doolen, and S. Chen, ''Calculations of longitudinal and transverse velocity structure functions using a vortex model of isotropic turbulence,'' Phys. Fluids **11**, 3743 (1999).
[37]T. Zhou and R. A. Antonia, ''Reynolds number dependence of the small-scale structure of grid turbulence,'' J. Fluid Mech. **406**, 81 (2000).
[38]A. Noullez, G. Wallace, W. Lempert, R. B. Miles, and U. Frisch, ''Transverse velocity increments in turbulent flow using the RELIEF technique,'' J. Fluid Mech. **339**, 287 (1997).
[39]V. S. L'vov, E. Podivilov, and I. Procaccia, ''Invariants for correlations of velocity differences in turbulent fields,'' Phys. Rev. Lett. **79**, 2050 (1997).
[40]G. He, S. Chen, R. H. Kraichnan, R. Zhang, and Y. Zhou, ''Statistics of dissipation and enstrophy induced by localized vorticies,'' Phys. Rev. Lett. **81**, 4636 (1998).
[41]A. Bershadskii, T. Nakano, D. Fukayama, and T. Gotoh, ''Local multifractal thermodynamics of 3D turbulence,'' Eur. Phys. J. B **18**, 95 (2000).
[42]D. Fukayama, Ph.D. thesis, Chuo University, 2001.
[43]T. Gotoh and D. Fukayama, ''Pressure spectrum in homogeneous turbulence,'' Phys. Rev. Lett. **86**, 3775 (2001).
[44]D. Fukayama, T. Nakano, A. Bershadskii, and T. Gotoh, ''Local properties of extended self-similarity in three-dimensional turbulence,'' Phys. Rev. E **64**, 016304 (2001).
[45]T. Nakano, D. Fukayama, A. Bershadskii, and T. Gotoh, ''Stretched log-normal distribution and ESS in 3D turbulence,'' J. Phys. Soc. Jpn. (submitted).
[46]C. W. Van Atta and R. A. Antonia, ''Reynolds number dependence of skewness and flatness factors of turbulent velocity derivatives,'' Phys. Fluids **23**, 252 (1980).
[47]R. A. Antonia and B. R. Pearson, ''Effect of initial conditions on the mean energy dissipation rate and the scaling experiment,'' Phys. Rev. E **62**, 8086 (2000).
[48]T. Gotoh and R. H. Kraichnan, ''Statistics of decaying Burgers turbulence,'' Phys. Fluids A **5**, 445 (1993).
[49]T. Gotoh, ''Probability density functions in steady-state Burgers turbulence,'' Phys. Fluids **11**, 2143 (1999).
[50]J. Jiménez, ''Turbulent velocity fluctuations need not be Gaussian,'' J. Fluid Mech. **376**, 139 (1998).
[51]E. Barkovsky, G. Falkovich, I. Kolokolov, and V. Lebedev, ''Intermittency of Burger's turbulence,'' Phys. Rev. Lett. **78**, 1452 (1997).
[52]G. Falkovich and V. Levedev, ''Single-point velocity distribution in turbulence,'' Phys. Rev. Lett. **79**, 4159 (1997).
[53]R. Benzi, L. Biferale, G. Paladin, A. Vulpiani, and M. Vergassola, ''Multifractality in the statistics of the velocity gradients in turbulence,'' Phys. Rev. Lett. **67**, 2299 (1991).
[54]R. J. Hill, ''Equations relating structure functions of all orders,'' J. Fluid Mech. **434**, 379 (2001).
[55]E. A. Novikov, ''Functionals and the random-force method in turbulence theory,'' Zh. Eksp. Teor. Fiz. **47**, 1919 (1964) [Sov. Phys. JETP **20**, 1290 (1965)].
[56]F. Moisy, P. Tabeling, and H. Willaime, ''Kolmogorov equation in a fully developed turbulence experiment,'' Phys. Rev. Lett. **82**, 3994 (1999).
[57]E. Lindborg, ''A note on Kolmogorov's third-order structure-function law, the local isotropy hypothesis and the pressure-velocity correlation,'' J. Fluid Mech. **326**, 343 (1996).
[58]R. Hill, ''Applicability of Kolmogorov's and Monin's equation of turbulence,'' J. Fluid Mech. **353**, 67 (1999).
[59]K. R. Sreenivasan, S. I. Vainshtein, R. Bhiladvala, I. San Gil, S. Chen, and N. Cao, ''Asymmetry of velocity increments in fully developed turbulence and the scaling of low-order moments,'' Phys. Rev. Lett. **77**, 1488 (1996).
[60]R. A. Antonia, M. Ould-Rouis, F. Anselmet, and T. Zhou, ''Analogy between prediction of Kolmogorov and Yaglom,'' J. Fluid Mech. **332**, 395 (1997).
[61]D. Fukayama, T. Oyamada, T. Nakano, T. Gotoh, and K. Yamamoto, ''Longitudinal structure functions in decaying and forced turbulence,'' J. Phys. Soc. Jpn. **69**, 701 (2000).
[62]R. A. Antonia, T. Zhou, L. Danaila, and F. Anselmet, ''Streamwise inhomogeneity of decaying grid turbulence,'' Phys. Fluids **12**, 3086 (2000).
[63]L. Danaila, F. Anselmet, T. Zhou, and R. A. Antonia, ''Turbulent energy scale budget equations in a fully developed channel flow,'' J. Fluid Mech. **430**, 87 (2001).
[64]S. I. Vainshtein and K. R. Sreenivasan, ''Kolmogorov's 4/5 law and intermittency in turbulence,'' Phys. Rev. Lett. **73**, 3085 (1994).
[65]L. Danaila, F. Anselmet, T. Zhou, and R. A. Antonia, ''A generalization of Yaglom's equation which accounts for the large-scale forcing in heated decaying turbulence,'' J. Fluid Mech. **391**, 359 (1999).

[66]J. Qian, ''Inertial range and the finite Reynolds number effect of turbulence,'' Phys. Rev. E **55**, 337 (1997).
[67]E. Lindborg, ''Correction to the four-fifth law due to variations of the dissipation,'' Phys. Fluids **11**, 510 (1999).
[68]J. Qian, ''Slow decay of the finite Reynolds number effect of turbulence,'' Phys. Rev. E **60**, 3409 (1999).
[69]T. Lundgren, ''Kolmogorov two-thirds law by matched asymptotic expansion,'' Phys. Fluids **14**, 638 (2002).
[70]Z. S. She and E. Lévêque, ''Universal scaling laws in fully developed turbulence,'' Phys. Rev. Lett. **72**, 336 (1994).
[71]R. Kerr, M. Meneguzzi, and T. Gotoh, ''An inertial range crossover in structure functions,'' Phys. Fluids **13**, 1985 (2001).
[72]V. Yakhot, ''Mean-field approximation and a small parameter in turbulence theory,'' Phys. Rev. E **63**, 026307 (2001).
[73]T. Arimitsu and N. Arimitsu, ''Analysis of fully developed turbulence in terms of Tsallis statistics,'' Phys. Rev. E **61**, 3237 (2000).
[74]T. Arimitsu and N. Arimitsu, ''Analysis of turbulence by statistics based on generalized entropies,'' Physica A **295**, 177 (2001).
[75]M. Nelkin and S. Chen, ''The scaling of pressure in isotropic turbulence,'' Phys. Fluids **10**, 2119 (1998).
[76]R. J. Hill and J. M. Wilczak, ''Pressure structure functions and spectra for locally isotropic turbulence,'' J. Fluid Mech. **296**, 247 (1995).
[77]R. J. Hill and O. N. Boratav, ''Next order structure-function equations,'' Phys. Fluids **13**, 276 (2001).
[78]S. Kurien and K. R. Sreenivasan, ''Dynamical equations for high-order structure functions, and a comparison of a mean field theory with experiments in three dimensional turbulence,'' arXiv:nlin.CD/0105046 May 2001.
[79]E. Aurell, U. Frisch, J. Lutsko, and M. Vergassola, ''On the multifractal properties of the energy dissipation derived from turbulence data,'' J. Fluid Mech. **238**, 467 (1992).
[80]T. Gotoh, ''Inertial range statistics of Burgers turbulence,'' Phys. Fluids **6**, 3985 (1994).
[81]T. Gotoh, T. Nakano, and N. Takahashi, ''Probability density function for velocity from the view point of conditional average,'' Research Inst. for Applied Mech. Report, *Turbulence Phenomena and Related Topics* (in Japanese), 10ME-S4, Kyushu University, April 1999, pp. 137.
[82]T. Ochiai, Master thesis, Nagoya Institute of Technology, 2001.
[83]T. Miyauchi and M. Tanahashi, ''Coherent fine scale structure in turbulence,'' *Proceedings of IUTAM Symposium on Geometry and Statistics of Turbulence*, edited by T. Kambe (Kluwer, New York, 2001).
[84]R. A. Antonia, B. R. Satyaprakash, and A. J. Chambers, ''Reynolds number dependence of velocity structure functions in turbulent shear flows,'' Phys. Fluids **25**, 29 (1982).
[85]R. A. Antonia, B. R. Pearson, and T. Zhou, ''Reynolds number dependence of second-order velocity structure functions,'' Phys. Fluids **12**, 3000 (2000).
[86]V. S. L'vov and I. Procaccia, ''Viscous lengths in hydrodynamic turbulence are anomalous scaling functions,'' Phys. Rev. Lett. **77**, 3541 (1996).
[87]M. Nelkin, ''Enstrophy and dissipation must have the same scaling exponent in the high Reynolds number limit of fluid turbulence,'' Phys. Fluids **11**, 2202 (1999).